iScience

CellPress
OPEN ACCESS

Article

Bone erosion in inflammatory arthritis is attenuated by *Trichinella spiralis* through inhibiting M1 monocyte/macrophage polarization

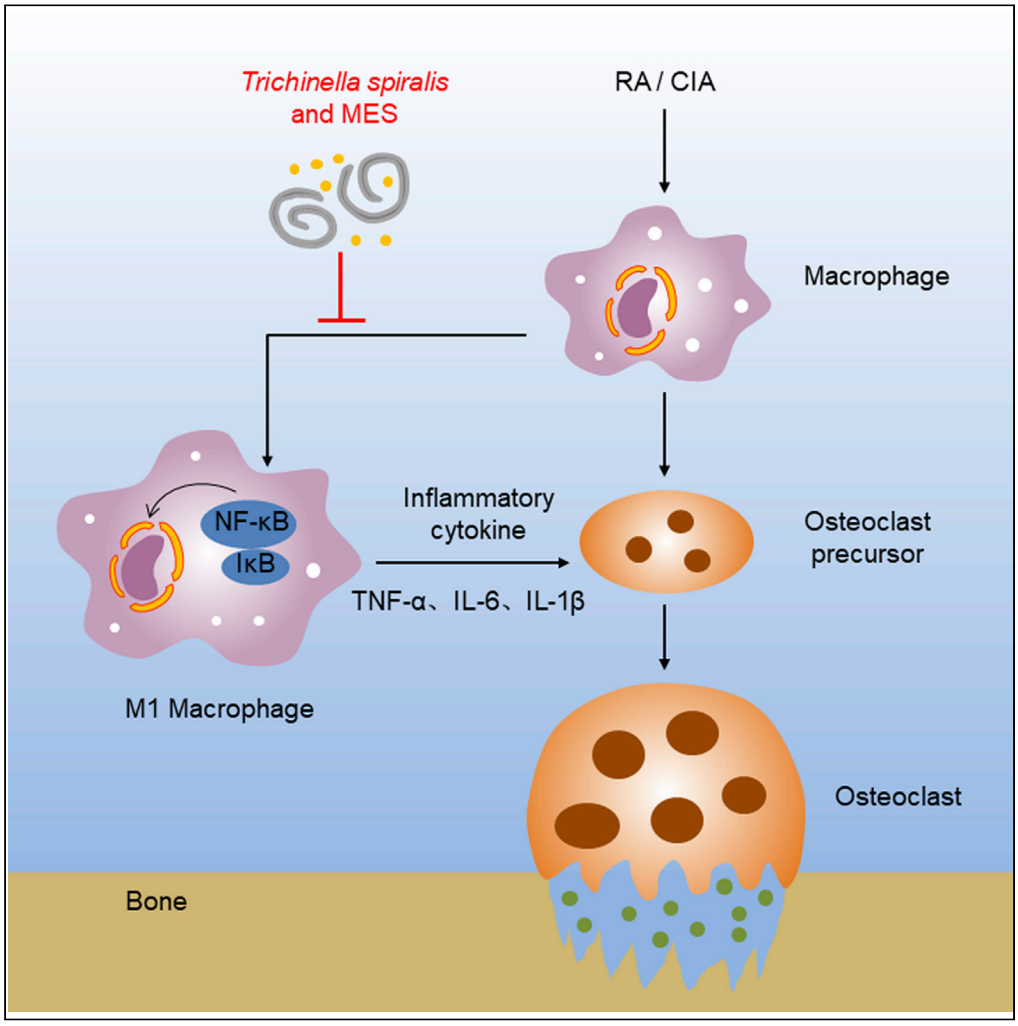

Yuli Cheng, Yan Yu, Qinghui Zhuang, ..., Jingjing Huang, Junfeng Hao, Xinping Zhu

zhuxping@ccmu.edu.cn (X.Z.)
chengyl@ccmu.edu.cn (Y.C.)

Highlights

Trichinella spiralis and MES attenuate bone erosion in inflammatory arthritis in mice

M1 polarization positively correlates osteoclastogenesis in RA patients and CIA mice

MES inhibit M1 polarization which is positively correlates with osteoclast formation

MES attenuate osteoclast differentiation through inhibiting the activation of NF-κB

Cheng et al., iScience *25*, 103979
March 18, 2022
https://doi.org/10.1016/j.isci.2022.103979

iScience

CellPress
OPEN ACCESS

Article

Bone erosion in inflammatory arthritis is attenuated by *Trichinella spiralis* through inhibiting M1 monocyte/macrophage polarization

Yuli Cheng,[1,5,*] Yan Yu,[1,5] Qinghui Zhuang,[1,5] Lei Wang,[2] Bin Zhan,[3] Suqin Du,[1] Yiqi Liu,[1] Jingjing Huang,[1] Junfeng Hao,[4] and Xinping Zhu[1,6,*]

SUMMARY

Helminths and helminth-derived products hold promise for treating joint bone erosion in rheumatoid arthritis (RA). However, the mechanisms of helminths ameliorating the osteoclastic bone destruction are incompletely understood. Here, we report that *Trichinella spiralis* infection or treatment with the excreted/secreted products of *T. spiralis* muscle larvae (MES) attenuated bone erosion and osteoclastogenesis in mice with collage-induced arthritis (CIA) through inhibiting M1 monocyte/macrophage polarization and the production of M1-related proinflammatory cytokines. *In vitro*, MES inhibited LPS-induced M1 macrophage activation while promoting IL-4-induced M2 macrophage polarization. Same effects of MES were also observed in monocytes derived from RA patients, wherein MES treatment suppressed LPS-induced M1 cytokine production. Moreover, MES treatment attenuated LPS and RANKL co-stimulated osteoclast differentiation from the RAW264.7 macrophages through inhibiting activation of the NF-κB rather than MAPK pathway. This study provides insight into the M1 subset as a potential target for helminths to alleviate osteoclastic bone destruction in RA.

INTRODUCTION

Rheumatoid arthritis (RA) is a chronic inflammatory disease characterized by synovitis and progressive cartilage and bone destruction, ultimately leading to joint deformity and disability (Scott et al., 2010). Irreversible periarticular bone erosion is a hallmark of RA and is associated with disease severity and functional deterioration (Schett and Gravallese, 2012). Histopathological characterization of bone erosion in patients with RA and animal models of inflammatory arthritis, such as collagen-induced arthritis (CIA), has provided strong evidence of an important role for bone-resorbing osteoclasts (OCs) in the structural joint damage associated with inflammatory arthritis (Catrina et al., 2017; Mbalaviele et al., 2017). OCs are differentiated from monocytes and macrophages through the stimulation of receptor activator for nuclear factor kappa-B ligand (RANKL) in the presence of macrophage colony stimulating factor (M-CSF). Upon RANKL binding to its receptor RANK, a variety of downstream signaling pathways responsible for OC differentiation are activated. The early phase osteoclastogenic signaling, governed by factors such as mitogen-activated protein kinases (MAPKs) and the receptor activator of nuclear factor (NF-κB), culminates in the activation of nuclear factor of activated T cells, cytoplasmic 1 (NFATc1), a master regulator for osteoclastogenesis (Boyle et al., 2003). In the late phase of osteoclastogenesis, NFATc1 transcriptionally controls osteoclast terminal differentiation by activating a number of OCs specific genes such as encoding tartrate-resistant acid phosphatase (TRAP), cathepsin K, calcitonin receptor (Kim and Kim, 2014).

Increasing evidence has indicated that macrophage infiltration into the synovium is involved in the pathogenesis of RA and correlates with the degree of joint erosion (Udalova et al., 2016). These macrophages are derived primarily from circulating monocytes. These monocytes can be differentiated into proinflammatory M1 or anti-inflammatory M2 macrophage subtypes under different conditions (Italiani and Boraschi, 2014). Macrophages/monocytes are polarized toward the M1 subtype under the stimulation of infectious microorganism-related molecules such as lipopolysaccharide (LPS) or inflammatory cytokines such as interferon-gamma (IFN-γ). M1 macrophages, also called classically activated macrophages, can produce toxic

[1]Department of Medical Microbiology and Parasitology, School of Basic Medical Sciences, Capital Medical University, Beijing 100069, PR China

[2]Beijing Institute of Tropical Medicine, Beijing Friendship Hospital, Capital Medical University, Beijing 100050, PR China

[3]Departments of Pediatrics and Molecular Virology and Microbiology, National School of Tropical Medicine, Baylor College of Medicine, Houston, TX 77030, USA

[4]Core Facility for Protein Research, Institute of Biophysics, Chinese Academy of Science, Beijing 100101, PR China

[5]These authors contributed equally

[6]Lead contact

*Correspondence: zhuxping@ccmu.edu.cn (X.Z.), chengyl@ccmu.edu.cn (Y.C.)

https://doi.org/10.1016/j.isci.2022.103979

effector molecules such as reactive oxygen species and nitric oxide, as well as proinflammatory cytokines such as interleukin (IL)-1β, tumor necrosis factor (TNF), and IL-6 to promote inflammation and the clearance of invading pathogens. Conversely, M2 macrophages, also known as alternatively activated macrophages, are associated with responses to Th2 cytokines such as IL-4 and IL-13 and secrete large amounts of anti-inflammatory cytokines (mainly IL-10 and transforming growth factor (TGF)-β) to reduce inflammation and promote vasculogenesis, wound healing, and tissue remodeling and repair (Orecchioni et al., 2019). Hence, the regulation of monocyte/macrophage M1/M2 polarization is essential for balancing tissue homeostasis and driving or resolving inflammation in most disease processes (Atri et al., 2018).

It has been demonstrated that the M1/M2 macrophage ratio is markedly increased along with the levels of TNF-α in inflamed synovial tissue of RA patients, indicating that M1 macrophages and secreted inflammatory cytokines may be involved in RA progression and play a pathogenic role in this disease (Tardito et al., 2019). Clinical studies have shown that OC differentiation is closely related to an M1/M2 phenotype imbalance among blood monocytes. RA patients with a higher M1/M2 ratio reportedly display a greater number of OCs, suggesting that an increase in M1 polarization is correlated with OC formation and disease progression (Fukui et al., 2017). Although the mechanism involved in how an increased M1/M2 ratio leads to OC overactivation remains unclear, the development of biological agents that can promote macrophage polarization toward an anti-inflammatory response has been proposed as a therapeutic strategy for preventing bone destruction and reducing disease severity in RA patients (Fernandes et al., 2020).

Over the past few decades, helminth infections or helminth-derived products have been widely reported to exhibit a substantial immunomodulatory potential in limiting the severity of chronic inflammation-associated diseases (CIADs) (Sobotkova et al., 2019). Despite the organismal complexity of different helminth species, helminth-induced type-2 immune responses are generally thought to exert inhibitory effects in inflammatory and/or autoimmune disorders (Douglas et al., 2021; Harris and Loke, 2017). Studies in animal models have demonstrated that intentional exposure to helminths or helminth-derived products can effectively alleviate inflammatory arthritis by inducing Th2 responses or $FOXP3^+$ T regulatory cells (Barranco, 2016; Chen et al., 2016). Recent studies have shown that helminth infections or helminth products are not only capable of suppressing arthritic inflammation but can also protect against arthritis-associated bone erosion in animal models (Doonan et al., 2018; Khan et al., 2020; Sarter et al., 2017). Although macrophages play a crucial role in osteoclastic activity, the mechanism that helminths target macrophage to inhibit bone erosion in inflammatory arthritis is not well understood.

T. spiralis is an intestinal and tissue-dwelling nematode that secretes various molecules to modulate the immune response of its host as a survival strategy. Infection with this nematode or *Trichinella*-secreted proteins has been employed for the treatment of many hyperimmune-associated disorders in experimental studies (Wang et al., 2020; Yang et al., 2020). We have previously demonstrated that *T. spiralis* infection can suppress arthritis by regulating $CD4^+$T-cell subsets (Cheng et al., 2018). In the present study, we demonstrate that *T. spiralis* infection significantly alleviates bone destruction through inhibiting M1 polarization and the production of M1-related inflammatory cytokines. Our data further indicate that the excretory/secretory products from muscle larvae of *T. spiralis* (MES) may contribute to the inhibitory effect of *T. spiralis* on bone erosion aroused from inflammatory arthritis.

RESULTS

T. spiralis infection reduces bone destruction and inhibits osteoclastogenesis in the joints of mice with CIA

To determine whether *T. spiralis* infection attenuates bone destruction in mice with CIA, mice were infected with *T. spiralis* 14 days before disease induction. HE staining showed that the larvae of *T. spiralis* had already reached the skeletal muscle at day 28 after oral infection (Figure S1). Micro-CT was used to scan the paws of mice after induction. Reconstructed 3D images captured during the analysis showed the presence of severe bone erosion in CIA mice, which was not seen in normal control mice; however, bone erosion was significantly attenuated in mice infected with *T. spiralis* before the induction of CIA, as evidenced by the reduction in the bone volume/total volume (BV/TV) and trabecular thickness (Tb.Th) in infected mice (Figure 1A). Given that OCs are crucial effectors of bone resorption, we next measured the number of TRAP-positive OCs in the paw sections of mice from each group. Histological examination showed that the number of OCs was significantly lower in *T. spiralis*-infected mice with CIA than in uninfected CIA model

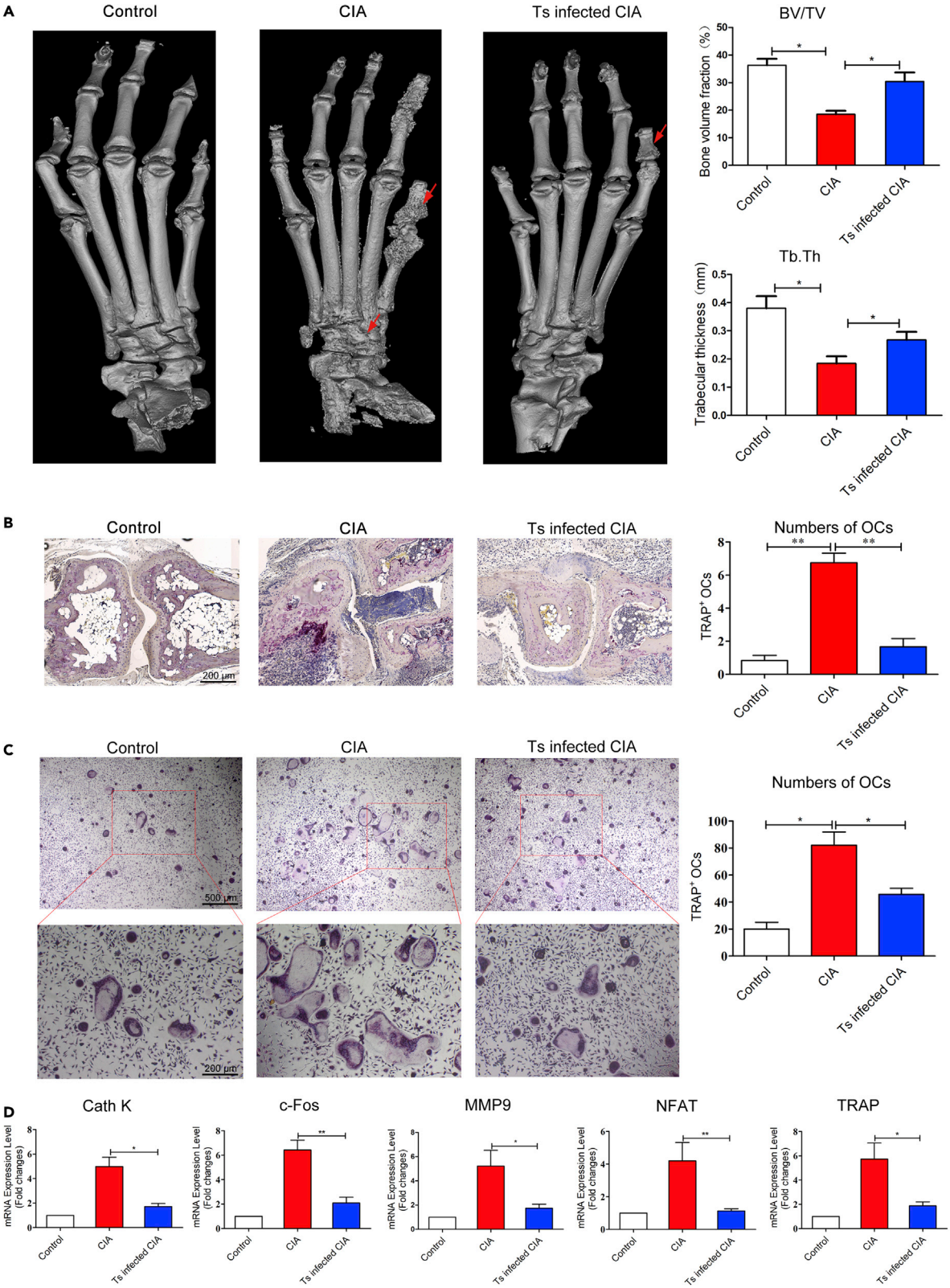
A
Control
CIA
Ts infected CIA
BV/TV
Bone volume fraction (%)
Tb.Th
Trabecular thickness (mm)
B
Control
CIA
Ts infected CIA
200 μm
Numbers of OCs
TRAP+ OCs
C
Control
CIA
Ts infected CIA
500 μm
200 μm
Numbers of OCs
TRAP+ OCs
D
Cath K
c-Fos
MMP9
NFAT
TRAP
mRNA Expression Level (Fold changes)

Figure 1. *Trichinella spiralis* infection alleviates bone erosion and inhibits osteoclastogenesis in the joints of mice with collagen-induced arthritis (CIA)

(A) Representative 3D images of the hind paws from mice of control, CIA or *T. spiralis* (Ts) infected CIA groups (left panel). Significant bone erosion and disruption was pointed by red arrows. The bone volume/total volume ratio (BV/TV) and trabecular thickness (Tb.Th) were quantified in the different groups of mice (right panel).

(B) Joint synovium sections were stained with TRAP (left panel, scale bar, 200 μm) and the numbers of osteoclasts (OCs) (red arrows) per view field were counted using ImageJ software (right panel).

(C) Peripheral blood mononuclear cells (PBMCs) from the different groups of mice were stimulated with murine RANKL (50 ng/mL) and M-CSF (30 ng/mL) for 7 days and then stained with TRAP. The numbers of TRAP-stained multinucleated OCs (≥3 nuclei, pointed by red arrows) (left panel, scale bar, 500 μm and 200 μm) were counted per field of view (right panel).

(D) Total RNA was extracted from M-CSF- and RANKL-stimulated monocytes isolated from PBMCs and the relative gene expression levels of TRAP, NFAT, MMP-9, c-Fos, and cathepsin K were measured by RT-qPCR. Data are expressed as the means ± SEM from three independent experiments (n = 5 mice per group). *p <0.05; **p <0.01.

mice (Figure 1B). These data suggested that *T. spiralis* infection inhibits arthritic damage and bone destruction in the paws of mice with CIA through inhibiting OC formation in affected joints.

To investigate whether *T. spiralis* infection affects the ability of monocytes to differentiate into OCs in mice with CIA, we next evaluated the RANKL-induced osteoclastic differentiation of blood monocytes derived from the three groups of mice. Monocytes were cultured in the presence of M-CSF and RANKL for 7 days, after which TRAP staining was performed to measure OC differentiation and formation. As shown in Figure 1C, the number of $TRAP^+$ cells (≥3 nuclei and ≥100 μm in diameter) was significantly increased in CIA model mice compared with that in normal control mice; however, *T. spiralis* infection reversed these results. We next assessed the mRNA levels of osteoclastogenesis-related genes in the paws of the various experimental groups. The transcript levels of cathepsin K, c-Fos, MMP-9, NFAT, and TRAP were significantly increased in CIA model mice compared with those of control mice; however, these increases were significantly attenuated in *T. spiralis*-infected CIA model mice (Figure 1D). Combined, these results suggested that *T. spiralis* infection inhibits OC differentiation in the paws of mice with induced CIA.

T. spiralis infection inhibits monocyte/macrophage M1 polarization

The balance between M1 and M2 polarization has been shown to play a crucial role in RA progression. To investigate whether *T. spiralis* infection affects monocyte polarization in mice with CIA, the numbers of M1 ($CD11b^+CD115^+$, $NOS2^+$) and M2 ($CD11b^+CD115^+$, $CD206^+$) monocytes among peripheral blood mononuclear cells (PBMCs) were determined by flow cytometry. As shown in Figures 2A and 2B, compared with normal controls, the percentage of macrophages displaying the M1 phenotype among $CD115^+$ monocytes was significantly higher in CIA model mice, whereas no difference was seen for the percentage of the M2 phenotype. Additionally, mice with CIA showed a significantly higher M1/M2 ratio compared with that in normal control mice. *T. spiralis* infection significantly reduced the M1 monocyte count, but had little effect on that of M2 monocytes in mice with CIA, leading to a significantly lower M1/M2 ratio. Similar changes were observed in peritoneal macrophages ($F4/80^+CD11b^+$) collected from the different groups of mice, namely, M1 polarization (NOS2) was significantly increased in mice with CIA, but significantly reduced upon *T. spiralis* infection (Figures 2C and 2D). We further analyzed the phenotypes of macrophages in the synovium of joints using immunofluorescence staining of hind paw sections. As shown in Figures 2E and 2F, the number of $F4/80^+NOS2^+$ M1 macrophages was significantly increased in mice with CIA compared with that in normal mice, while *T. spiralis* infection significantly decreased the M1 population. Again, no significant change in the numbers of M2 macrophages ($F4/80^+CD206^+$) was observed among the three groups. These data clearly demonstrated that *T. spiralis* infection reduces CIA-induced M1 polarization but has little effect on the M2 population. Interestingly, the percentages of cells with the M1 phenotype in blood and in joint synovium of CIA mice with or without *T. spiralis* infection were positively correlated with the numbers of OCs in the joints (Figures 2G and 2H), indicating that M1 polarization is related to OC differentiation in mice with CIA, and that *T. spiralis* infection attenuates osteoclastogenesis in these model mice by reducing the M1 population.

T. spiralis infection suppresses proinflammatory cytokine production in mice with CIA

To investigate the effect of *T. spiralis* infection on the systemic proinflammatory cytokine response to CIA, we evaluated the serum cytokine profile in the three groups of mice using multiplex xMAP assay. The results showed that a total of 21 cytokines, including the proinflammatory cytokines IL-1β, IL-6, TNF-α, IL-12, IL-17,

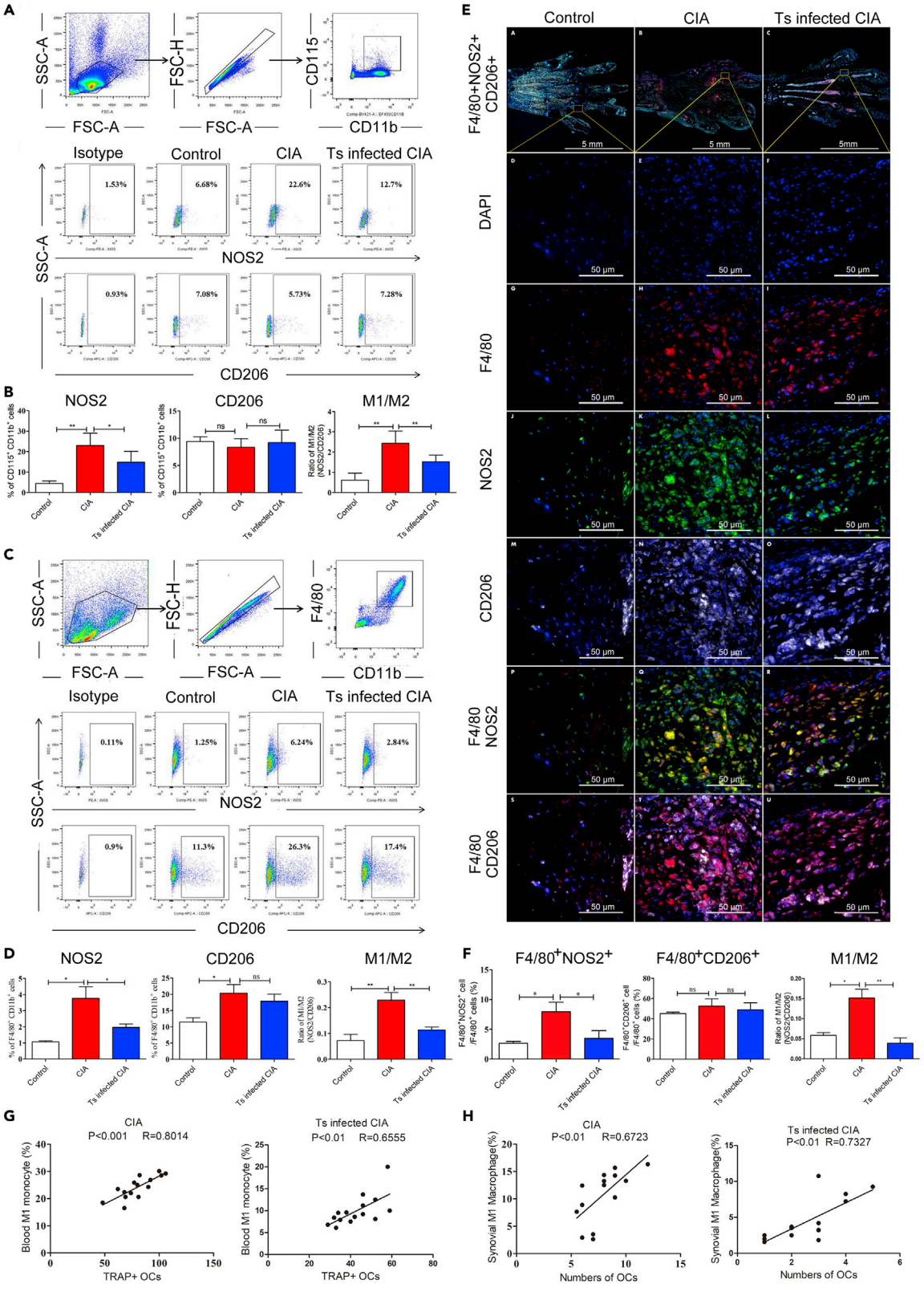
A
SSC-A
FSC-A
FSC-H
FSC-A
CD115
CD11b
Isotype
Control
CIA
Ts infected CIA
1.53%
6.68%
22.6%
12.7%
NOS2
0.93%
7.08%
5.73%
7.28%
CD206
B
NOS2
CD206
M1/M2
% of CD115+ CD11b+ cells
Ratio of M1/M2 (NOS2/CD206)
Control
CIA
Ts infected CIA
C
SSC-A
FSC-A
FSC-H
FSC-A
F4/80
CD11b
Isotype
Control
CIA
Ts infected CIA
0.11%
1.25%
6.24%
2.84%
NOS2
0.9%
11.3%
26.3%
17.4%
CD206
D
NOS2
CD206
M1/M2
% of F4/80+ CD11b+ cells
Ratio of M1/M2 (NOS2/CD206)
Control
CIA
Ts infected CIA
E
Control
CIA
Ts infected CIA
F4/80+NOS2+ CD206+
DAPI
F4/80
NOS2
CD206
F4/80 NOS2
F4/80 CD206
5 mm
50 μm
F
F4/80+NOS2+
F4/80+CD206+
M1/M2
F4/80+NOS2+ cell /F4/80+ cells (%)
F4/80+CD206+ cell /F4/80+ cells (%)
Ratio of M1/M2 (NOS2/CD206)
Control
CIA
Ts infected CIA
G
CIA
P<0.001 R=0.8014
Ts infected CIA
P<0.01 R=0.6555
Blood M1 monocyte (%)
TRAP+ OCs
H
CIA
P<0.01 R=0.6723
Ts infected CIA
P<0.01 R=0.7327
Synovial M1 Macrophage(%)
Numbers of OCs

Figure 2. *Trichinella spiralis* infection inhibits M1 macrophage polarization in mice with collagen-induced arthritis (CIA)

(A) Flow cytometry gating strategy to define $CD11b^+CD115^+$ monocytes among peripheral blood mononuclear cells (PBMCs) and representative dot plots showing the M1 ($NOS2^+$) and M2 ($CD206^+$) from mice of control, CIA and *T. spiralis* (Ts) infected CIA group.

(B) The percentage of M1 and M2 monocytes and the M1/M2 ratio in each group.

(C) Flow cytometry gating strategy to define $CD11b^+F4/80^+$ peritoneal macrophages and representative dot plots showing the M1 ($NOS2^+$) and M2 ($CD206^+$) from mice of each group.

(D) The percentages of M1 ($NOS2^+$) and M2 ($CD206^+$) macrophages and the M1/M2 ration in each group.

(E) Representative photomicrographs of multiplex immunofluorescence staining for M1 ($NOS2^+$, green) and M2 ($CD206^+$, white) in synovial macrophages ($F4/80^+$, red) on day 49 after the first immunization with type II collagen (CII). Nuclei were counterstained with DAPI (blue).

(F) The percentage of M1 and M2 macrophages and the M1/M2 ratio in the synovium of joints in each group.

(G) Spearman's correlation analysis for the numbers of osteoclasts (OCs) differentiated from blood monocytes and the proportion of M1 population in PBMCs from CIA mice with or without *T. spiralis* infection.

(H) Spearman's correlation analysis for the numbers of OCs in joint synovium sections and synovial macrophages of CIA mice with or without *T. spiralis* infection. Data are expressed as the means ± SEM from three independent experiments (n = 5 mice per group). *p <0.05; **p <0.01.

and GM-CSF, were significantly upregulated in mice with CIA; however, *T. spiralis* infection significantly reduced the levels of these six pro-inflammatory cytokines in the sera of mice with CIA, with IL-6 showing the most significant reduction ($p<0.01$). The anti-inflammatory cytokine IL-10 upregulated in mice with CIA was also decreased by *T. spiralis* infection but no significant difference was showed among the three groups. Infection with *T. spiralis* increased the serum level of eotaxin, consistent with eosinophil recruitment following helminth infection (Figure 3A, Table S1). To further investigate the effect of *T. spiralis* infection on macrophage-related cytokine production in the joints of CIA model mice, we next assessed the mRNA levels of IL-1β, TNF-α, IL-6, IL-12, and IL-10 in the synovium of joints of mice from the various groups. As shown in Figure 3B, *T. spiralis* infection led to a significant reduction in the expression levels of genes coding for proinflammatory cytokines (IL-1β, TNF-α, IL-6, and IL-12) in the synovium of joints from mice with CIA; however, the mRNA expression of anti-inflammatory cytokine IL-10 level was not significantly affected by *T. spiralis* infection. Similar cytokine profile changes were observed in macrophages collected from the peritoneal cavities of mice from the different groups. Following *in vitro* stimulation with LPS, peritoneal macrophages isolated from mice with CIA produced higher amounts of both the M1-associated cytokines IL-1β, IL-6, TNF-α and the M2-associated cytokine IL-10 than those collected from normal control mice; however, infection with *T. spiralis* significantly reduced the levels of these M1-related cytokines, whereas little change was seen in IL-10 levels (Figure 3C). These results suggested that infection with *T. spiralis* reduced the production of proinflammatory cytokines, indicative of the suppression of M1 polarization, and attenuated CIA-promoted bone erosion in the joints of mice.

Treatment with MES inhibits LPS-induced M1 polarization and enhances IL-4-induced M2 polarization in RAW264.7 cells

It is well established that MES plays an important role in the modulation of the host's immune system during chronic infection (Han et al., 2019; Kobpornchai et al., 2020). To determine the effect of MES on macrophage polarization, RAW264.7 macrophages were treated with MES *in vitro*. The results showed that compared with that in untreated controls, MES significantly reduced the LPS-stimulated mRNA expression of M1 phenotype-related factors such as iNOS, IL-6, TNF-α, IL-1β , and MCP-1; additionally, MES significantly enhanced the expression of the IL-4-induced M2 phenotype-related molecules CD206 and IL-10 in a dose-dependent manner (Figures 4A and 4B). The Arg-1 level was increased and peaked at the MES concentration of 4 μg/mL. Similarly, MES treatment reduced the LPS-induced production of the M1-related cytokines IL-6, TNF-α, and IL-1β, while dose-dependently enhancing the production of the M2 cytokine IL-10 (Figures 4C and 4D). Our findings confirmed that MES could effectively suppress LPS-induced M1 and enhance IL-4-induced M2 macrophage polarization *in vitro*. Notably, MES exerted similar inhibitory effects on M1 polarization as *T. spiralis* infection, but with a stronger ability to promote M2 polarization *in vitro* under non-inflammatory conditions.

Treatment with MES suppresses the inflammatory responses of blood monocytes derived from RA patients

After confirming the ability of MES to modulate monocyte/macrophage polarization in RAW264.7 cells, we next investigated the effects of MES on monocytes from PBMCs of RA patients. The general information of the total 26 enrolled patients showed a higher ratio of female patients (Table S2). First, we assessed the osteoclastogenic ability of monocytes derived from the blood of RA patients, and found a positive correlation between the M1 percentage in PBMCs and the number of OCs differentiated from blood monocytes

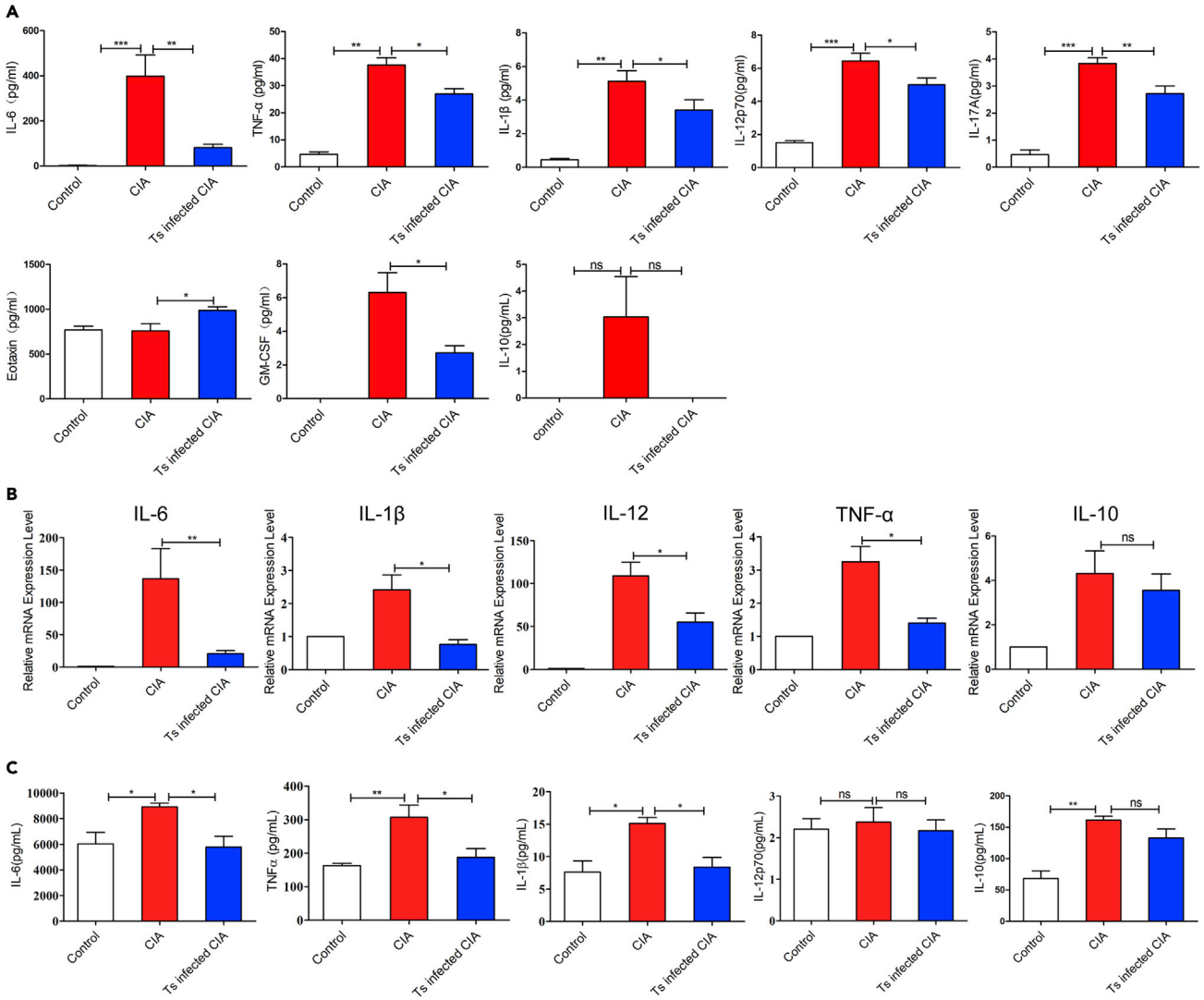

Figure 3. *Trichinella spiralis* infection suppresses proinflammatory cytokine production in mice with collagen-induced arthritis (CIA)

(A) Cytokine levels in the serum from mice of control, CIA and *T. spiralis* (Ts) infected CIA groups were analyzed by Luminex xMAP assay on day 49 after the first immunization with type II collagen (CII).

(B) The expression levels of proinflammatory cytokine-related genes in synovial tissues isolated from the hind paws of mice on day 49 were analyzed by RT-qPCR.

(C) M1-related cytokine levels were measured by ELISA in culture supernatants of macrophages collected from the peritoneal cavities of mice from the different groups and stimulated with 100 ng/mL lipopolysaccharide (LPS).Data are expressed as the means ± SEM from three independent experiments (n = 5 mice per group). *p <0.05; **p <0.01; ***p <0.001.

of the patients (Figures 5A and 5B). This result suggested that RA patients with higher proportion of M1 monocytes in peripheral blood are at a greater risk of excessive OC differentiation which leads to bone erosion. We further analyzed the effects of MES on the inflammatory response of blood monocytes from RA patients. For this, monocytes isolated from the peripheral blood of RA patients or healthy donors were pre-incubated with MES before LPS stimulation. The levels of the M1 cytokines IL-1β, IL-6, and TNF-α and those of the M2 cytokine IL-10 were measured in the culture supernatants. The results showed that blood monocytes from RA patients produced significantly higher levels of IL-1β, IL-6, TNF-α, and IL-10 compared with those from healthy donors with LPS stimulation; however, treatment with MES significantly reduced the levels of M1-related cytokines (IL-1β, IL-6, and TNF-α) secreted by monocytes derived from RA patients (Figure 6), but had little effect on IL-10. This result demonstrated that MES could suppress the inflammatory response of monocytes from RA patients.

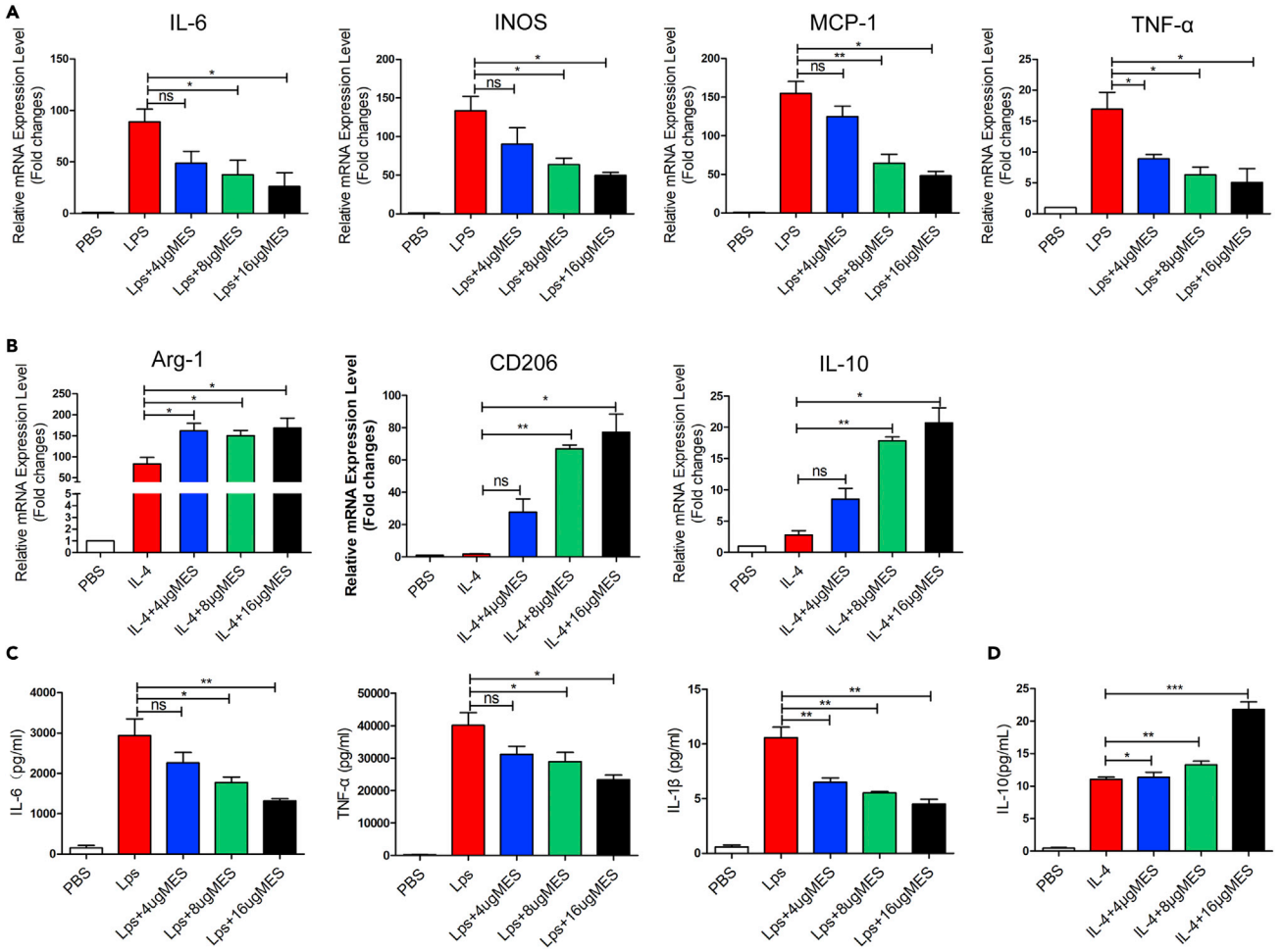

Figure 4. *Trichinella spiralis* MES inhibits LPS-induced M1 polarization and enhances IL-4-induced M2 polarization in RAW264.7 macrophages *in vitro*

RAW264.7 macrophages were pre-incubated with MES (4, 8, or 16 μg/mL) for 2 h prior to the addition of LPS (100 ng/mL) or IL-4 (20 ng/mL) to induce M1 or M2 polarization, respectively. The effect of MES on the expression of M1 phenotype- (A) or M2 phenotype-associated genes (B) was analyzed by RT-qPCR after 6 h of stimulation with LPS or IL-4. M1- (C) and M2-related (D) cytokine levels in the culture supernatants of RAW264.7 macrophages were measured by ELISA. The experiments were repeated three times. The data are expressed as means ±SEM*p <0.05; **p <0.01; ***p <0.001.

Treatment with MES reduces bone destruction and inhibits osteoclastogenesis in the joints of mice with CIA

After confirming the inhibitory effects of MES on proinflammatory cytokine production, we next determine whether MES reduces bone destruction aroused from CIA in mice. As shown in Figure 7A, mice were treated with MES before and during the CIA induction. Bone erosion was significantly attenuated in CIA mice treated with MES, as evidenced by the reduction in the bone volume/total volume (BV/TV) and trabecular thickness (Tb.Th) in MES treated CIA model mice (Figure 7B). Histological examination showed that the number of OCs was significantly lower in *T. spiralis*-infected mice with CIA than in untreated CIA model mice (Figure 7C). These data suggested that treatment with MES inhibits bone destruction and OC formation in affected joints of mice with CIA.

Treatment with MES suppresses LPS-enhanced osteoclast differentiation by inhibiting the activation of NF-κB pathway rather than MAPK pathway

Incubation of macrophage with soluble RANKL results in multinucleated, $TRAP^+$ OCs. To investigate the effect of M1 and M2 polarization on macrophage differentiating into OC, we first examined the effect of

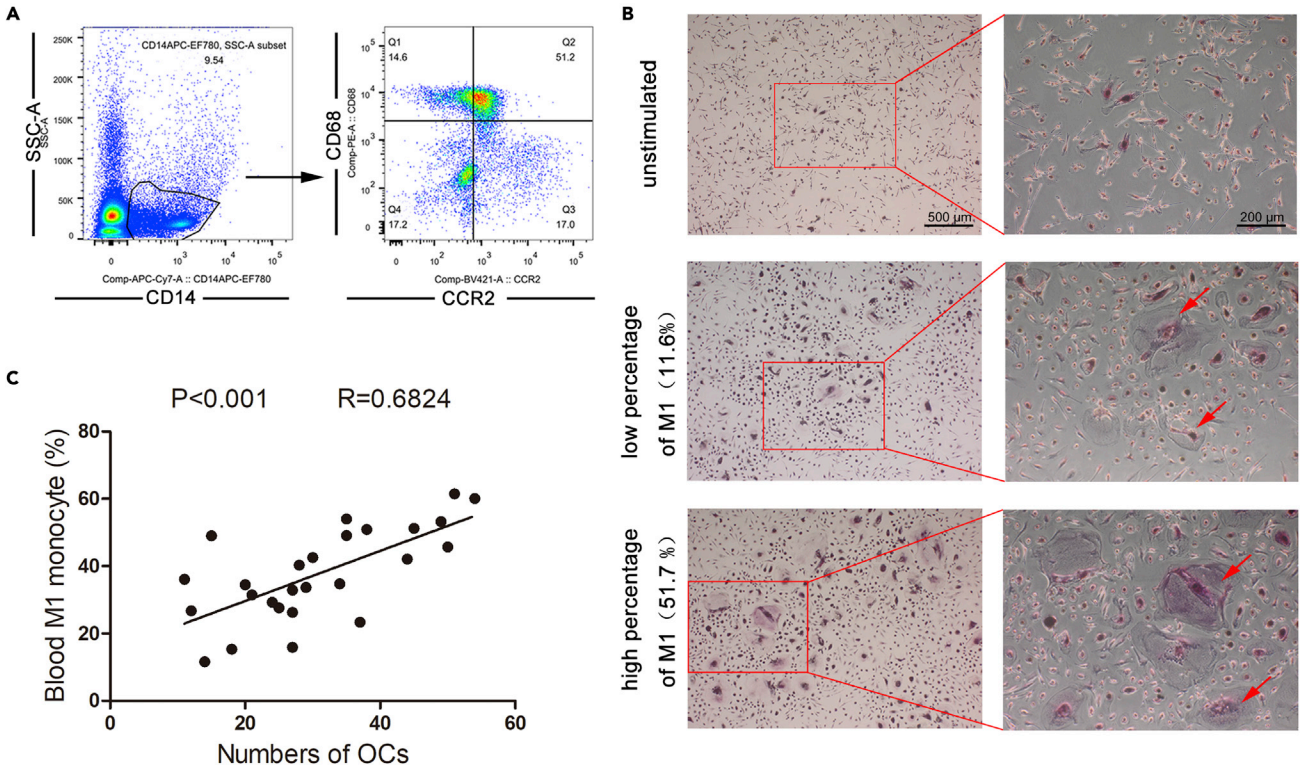

Figure 5. The percentage of M1 among blood monocytes positively correlated with the number of RANKL-induced osteoclasts (OCs) in rheumatoid arthritis (RA) patients

(A) M1 monocytes were defined as $CD14^+$, $CD68^+$, and $CCR2^+$.

(B) Blood monocytes from PBMCs of RA patients were stimulated with RANKL (50 ng/mL) and M-CSF (30 ng/mL) for 5 days to induce OCs and then stained with TRAP. Representative TRAP staining (scale bar, 500 μm and 200 μm) of the OCs (red arrows) differentiated from blood monocytes of RA patients with relatively higher or lower percentage of M1 were showed respectively.

(C) Spearman's correlation analysis for the numbers of OCs and the M1 percentage in blood monocytes of RA patients. The experiments were repeated three times. The data are expressed as means ±SEM.

LPS and IL-4 on RANKL-induced osteoclastogenesis in murine RAW264.7 macrophages respectively. As shown in Figure S2, the addition of LPS enhanced OC formation from RAW264.7 cells following RANKL stimulation, whereas IL-4 had little effect on RANKL-induced OC differentiation. Next, we examined the effects of MES on the LPS-stimulated, RANKL-induced differentiation of macrophages into OCs, and found that osteoclastogenesis from both bone marrow derived macrophages (BMMs) and RAW264.7 cells were significantly inhibited with MES treatment (Figures 8A and S3). To identify the effect of MES on expression of the osteoclastogenesis-related gene(s), we measured the gene expression levels of NFAT, c-Fos, cathepsin K, MMP-9, and TRAP by RT-qPCR. The results indicated that the expression levels of the LPS-enhanced and RANKL-induced genes related to osteoclastogenesis were significantly reduced by treatment with MES (Figure 8B).

To identify the signaling pathways through which MES regulates OC differentiation, we evaluated the effect of MES treatment on the activation of NF-κB and MAPK pathways. We found that treatment with MES reduced the phosphorylation levels of p65 and IκB, both of which are associated with the activation of NF-κB; however, it seems that *T. spiralis* MES had little effect on regulating the signaling of MAPK-related families such as ERK, JNK, and p38, under RANKL and LPS stimulation (Figure 8C), indicating that MES inhibits osteoclastogenesis through downregulating the activation of NF-κB rather than MAPK pathway. As NFATc1 is the master transcription factor responsible for the activation of OC-specific genes, we next determined whether pretreatment with MES affects the expression of NFATc1 in RAW264.7 cells. The results showed that NFATc1 expression was significantly reduced in RAW264.7 cells pre-incubated with MES followed by co-stimulation with RANKL and LPS (Figure 8D).

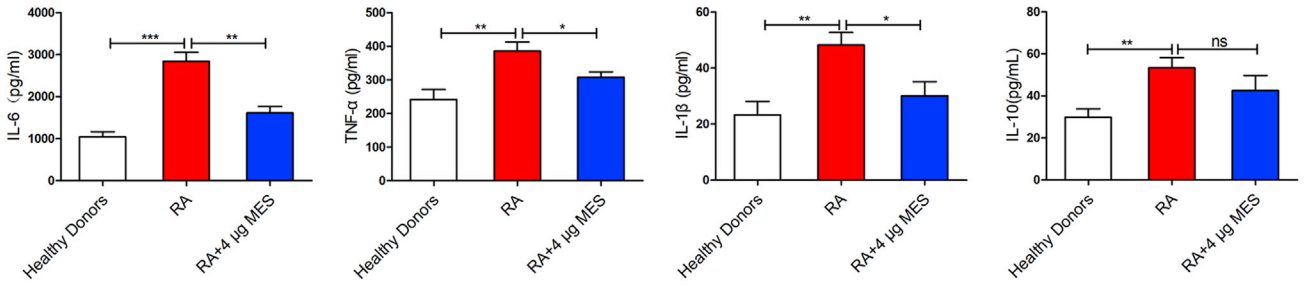

Figure 6. *Trichinella spiralis* MES suppresses proinflammatory cytokine production in blood monocytes from rheumatoid arthritis (RA) patients

Blood monocytes from RA patients were pre-incubated with MES (8 μg/mL) for 2 h prior to the stimulation with LPS (100 ng/mL). The levels of the cytokines IL-6, TNF-α, IL-1β, and IL-10 in the culture supernatants were measured by ELISA. The experiments were repeated three times. The data are expressed as means ±SEM*p <0.05, **p <0.01.

DISCUSSION

Bone destruction, the major pathological signature in RA, results from excess osteoclastic activity and leads to an imbalance in bone remodeling that favors resorption. Recent studies have indicated that helminths and helminth-derived products hold promise in reducing bone erosion associated with RA (Sobotkova et al., 2019). For instance, *Heligmosomoides polygyrus bakeri* (Hp) infection inhibits the arthritic bone loss and the excretory-secretory (ES) products from Hp directly suppress OC differentiation (Sarter et al., 2017). Here we show that *T. spiralis* infection attenuates the arthritis, evidenced by the reduced bone destruction and osteoclastogenesis observed in the joints of mice with CIA (Figures 1A–1C).

Helminths promote distinct phenotypes and functions in macrophages, reducing or preventing host immunopathology by inducing regulatory cell populations or diverting proinflammatory effector cells (Rolot and Dewals, 2018). This helminth-induced immunomodulation of macrophage polarization can be channeled toward developing new therapeutic approaches to treat immunoinflammatory diseases (Lechner et al., 2021; Steinfelder et al., 2016). In this study, we confirmed that M1 populations in PBMCs and the synovium of joints of CIA model mice were positively correlated with macrophage-derived OC differentiation (Figures 2A–2G). This association was also observed in monocytes obtained from PBMCs of RA patients (Figures 5A–5C), indicating the critical role of M1 monocytes in the osteoblastogenesis and pathogenesis of inflammatory arthritis. These results were consistent with clinical findings showing that RA patients had a higher M1/M2 ratio in peripheral blood and greater numbers of transformed OCs compared with those of healthy controls (Fukui et al., 2017). Moreover, we also found that infection with *T. spiralis* significantly reduced the numbers of M1 monocytes/macrophages which was associated with bone destruction and osteoblastogenesis in the affected joints. However, *T. spiralis* infection had only a limited effect on M2 population numbers both in PBMCs and the synovium of joints of mice with CIA. Together, these results suggested that *T. spiralis* infection attenuates inflammatory arthritis mainly through inhibiting M1 macrophage polarization.

In addition to a greater number of M1 macrophages, the proinflammatory environment created by the higher levels of M1 polarization also contributes to increased OC differentiation in RA patients (Nevius et al., 2016). RANKL is known to be a key inducer of osteoclastogenesis in the pathogenesis of RA (Mcdonald et al., 2021). Proinflammatory cytokines, including TNF-α, IL-17, IL-1β, and IL-6 have been reported to positively regulate RANKL expression in fibroblast-like synoviocytes (FLS) in both mice and humans with inflammatory arthritis (Tunyogi-Csapo et al., 2008). In this study, we confirmed that *T. spiralis* infection inhibited proinflammatory cytokine production in both serum and the synovium of mice with CIA, with IL-6 exhibiting the most significant reduction (Figures 3A, 3B and Table S1). IL-6, a major inflammatory cytokine, stimulates osteoclastogenesis through activating RANKL expression in FLSs in RA patients (Choe et al., 2013). These observations suggest that *T. spiralis* infection modulates the host immune response by inhibiting macrophage M1 polarization, and the production of M1-associated inflammatory cytokines especially IL-6, which may contribute to reduced bone erosion and osteoclastogenesis in mice with CIA. The inhibitory effect of *T. spiralis* infection on proinflammatory cytokine production was further confirmed in peritoneal macrophages from CIA model mice infected with *T. spiralis* (Figure 3C). These findings suggest that the modulation of macrophage polarization may contribute to a reduction in proinflammatory cytokine production in mice with CIA infected with *T. spiralis*. Concerning

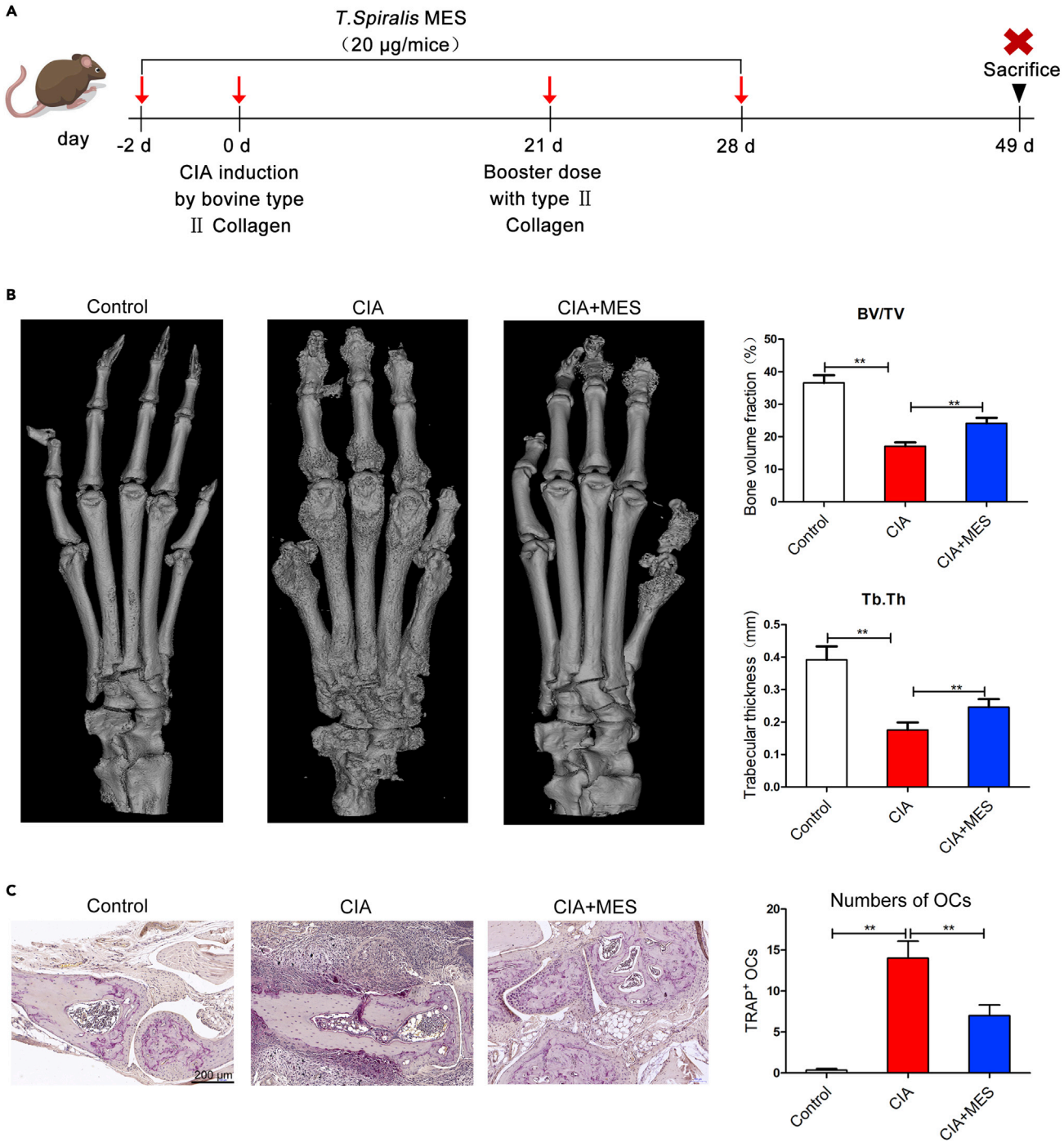

Figure 7. *Trichinella spiralis* MES alleviates bone erosion and inhibits osteoclastogenesis in the joints of mice with collagen-induced arthritis (CIA)

(A) The regimen of study including the induction of CIA and treatment with MES.

(B) Representative 3D images of the hind paws from mice of control, CIA or CIA + MES groups (left panel). The bone volume/total volume ratio (BV/TV) and trabecular thickness (Tb.Th) were quantified in the different groups of mice (right panel).

(C) Joint synovium sections were stained with TRAP (left panel, scale bar, 200 μm) and the numbers of osteoclasts (OCs) per view field were counted using ImageJ software (right panel). The results are expressed as the means ± SEM from three independent experiments (n = 5 mice per group). **p <0.01.

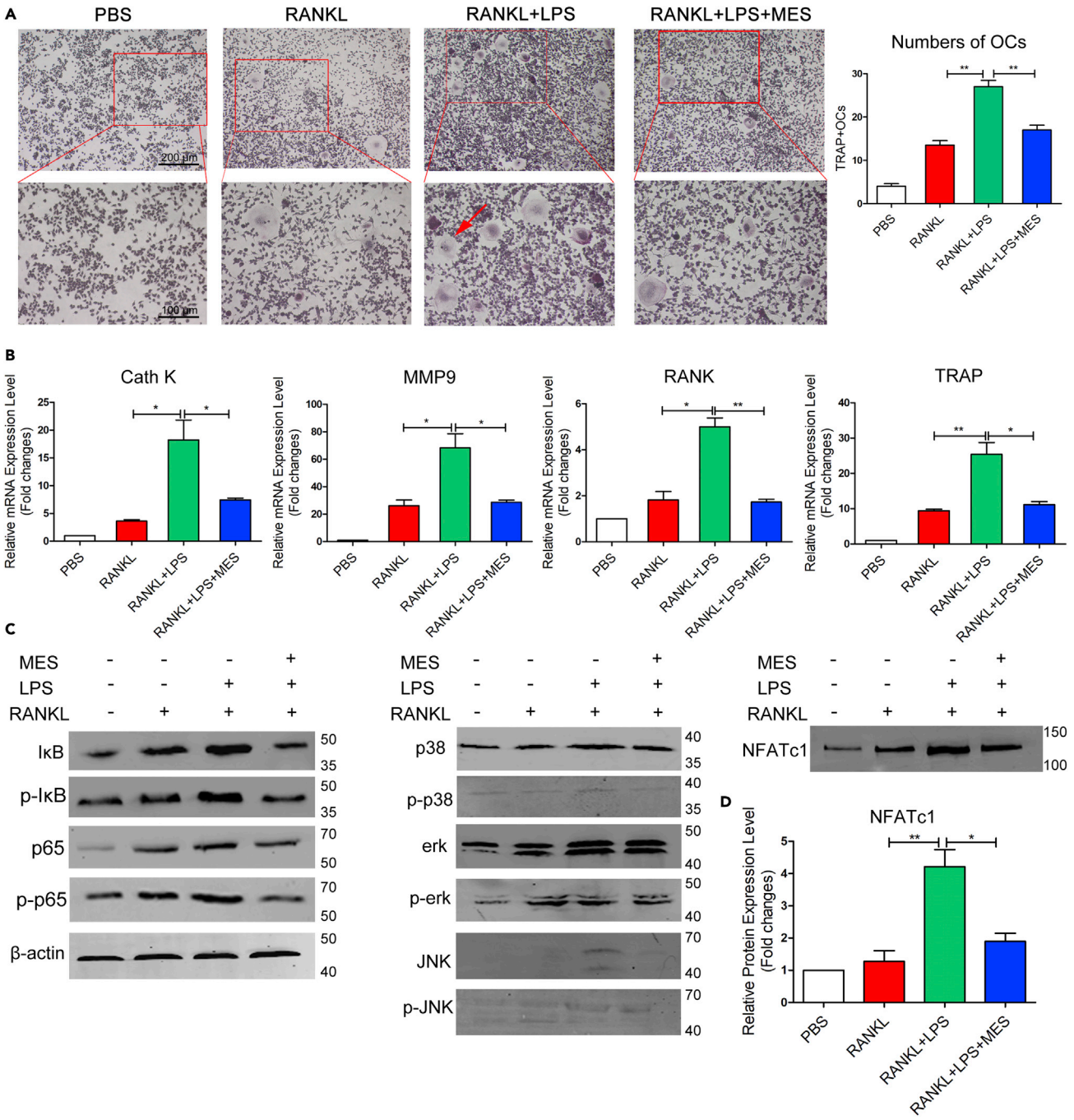

Figure 8. *Trichinella spiralis* MES suppresses LPS-enhanced and RANKL-induced osteoclast differentiation

RAW264.7 cells were first treated with MES (8 μg/mL) and LPS for 6 h, and then exposed to murine RANKL (50 ng/mL) for 5 days.

(A) Representative TRAP staining (left panel, scale bar, 200 μm and 100 μm) and the numbers of osteoclast (OCs) were counted per field of view (right panel) (OCs are indicated by red arrows).

(B) The mRNA levels of cathepsin k, MMP-9, RANK, and TRAP were detected by RT-qPCR.

(C) Equal amounts of RAW264.7 lysate (40 μg) were separated by 12% SDS–PAGE and then subjected to western blot with antibodies targeting molecules in the NF-κB and MAPK signaling pathways and NFAT. The results are expressed as the means ± SEM from three independent experiments. *p <0.05, **p <0.01.

the anti-inflammatory cytokine, induction of IL-10 often occurs together with pro-inflammatory cytokines, although pathways that induce IL-10 may actually negatively regulate these pro-inflammatory cytokines. Indeed, in this study, CIA induced IL-10 production in mice (Saraiva and O'Garra, 2010). Helminth infection also usually promotes the production of the regulatory cytokine IL-10 (Redpath et al., 2014; Schopf et al., 2002). However, *T. spiralis* infection had little effect on the IL-10 production in CIA mice, as indicated by the limited change of IL-10 levels after *T. spiralis* infection. This may be explained by the fact that the CIA-induced inflammatory environment strongly boosted IL-10 secretion, thereby offsetting the stimulation resulting from *T. spiralis* infection.

Helminths modulate the host immune system via direct contact or by secreting molecules that interact with the immune system of the host. It is well known that the excreted/secreted products (ES) of *T. spiralis* play an important role in modulating host immune system (Radovic et al., 2015). Accordingly, we tested the direct effect of the MES on macrophage polarization and the ensuing inflammatory profile, as the MES are the major products released during chronic *T. spiralis* infection. The results showed that the MES markedly inhibited LPS-induced M1 macrophage polarization and proinflammatory cytokine secretion, and enhanced IL-4-induced M2 macrophage polarization and the production of M2-associated cytokines, including IL-10, in RAW264.7 macrophages *in vitro*. Similar results were observed in monocytes isolated from PBMCs of RA patients. Incubation with MES significantly inhibited LPS-induced inflammatory responses in PBMCs derived from RA patients, including reducing the levels of the cytokines IL-6, TNF-α, and IL-1β in culture supernatants (Figure 6). Interestingly, IL-6 was also the most significantly downregulated cytokine in monocytes from RA patients following MES treatment, indicating that IL-6 is an important target of the ES products released by *T. spiralis* muscle larvae.

We further confirmed that MES treatment effectively reduced the bone erosion and the OC differentiation in mice with CIA (Figure 7), indicating the MES as inhibitors of OC differentiation and as potential biological products to treat CIA-induced bone loss. OCs are tissue-specific, multinucleated cells derived from monocyte/macrophage precursor cells at the bone surface (Ono and Nakashima, 2018). Helminth-derived products are reported to be capable of inhibiting OC differentiation while the mechanisms remain to be clarified. ES-62, a glycoprotein secreted by the rodent filarial nematode *Acanthocheilonema viteae* inhibits functional OC differentiation by induction of anti-oxidant response gene expression, thereby resulting in reduction of the reactive oxygen species production that is necessary for the osteoclastogenesis (Doonan et al., 2018). Additionally, a synthetic peptide of secretory protein from *Fasciola hepatica* inhibited the RANKL-induced differentiation of macrophages to OCs and lysosomal acidification of differentiated OCs by inhibiting the action of vATPase which trigger bone resorption (Khan et al., 2020). In this study, we found that LPS enhanced osteoclastogenesis from RAW264.7 macrophages upon RANKL stimulation *in vitro*, whereas IL-4 had little effect on RANKL-induced OC formation, indicative of a greater osteoclastogenic differentiation ability of M1 macrophages compared to M2 phenotype (Figure S2). Incubation with MES significantly inhibited osteoclastogenesis from both BMMs and RAW264.7 cells with LPS/RANKL co-stimulation (Figures S3,8A and 8B), possibly through inhibiting M1 polarization. NF-κB and MAPK activation are important early signaling events induced by RANKL. Our further analysis of the signaling pathways involved in osteoclastogenesis identified that MES inhibited osteoclastogenesis through inhibiting the activation of the NF-κB rather than MAPK signaling pathway (Figure 8C). NFATc1, a master transcription factor involved in the terminal differentiation of OCs and the transcriptional induction of associated genes downstream of NF-κB (Boyle et al., 2003; Lorenzo, 2017), was also downregulated by MES (Figure 8D).

In summary, in this study, we found that *T. spiralis* infection reduces bone erosion and osteoclastogenesis in mice by inhibiting M1 monocyte/macrophage polarization. MES play an important role in inhibiting osteoclastogenesis by attenuating M1 polarization in both RA patients and mice with CIA. Moreover, the NF-κB pathway in monocytes/macrophages is an important target on which the MES act to inhibit osteoclastogenesis. Our findings indicate that *T. spiralis* infection may exert its therapeutic effects on inflammatory arthritis through secreting ES products that interact with the immune system of the host and selectively inhibit M1 macrophage polarization. Our results increase the understanding of the mechanisms underlying the protective effects of MES on bone erosion in RA and provide insights into the development of MES as potential biological agents to treat bone erosion in this inflammatory disease. Further studies are needed to identify the specific protein(s) in MES that exert immunoregulatory functions, which may serve as biological agents for the treatment of bone erosion caused by inflammatory arthritis.

Limitations of the study

Our studies were mainly performed on mouse models. The differences in the pathophysiological and immunological characteristics between CIA model mice and RA patients may potentially limit the translational value of our conclusions. Although we found that MES suppress proinflammatory cytokine production in blood monocytes from RA patients, the effect of MES on OC differentiation of monocytes from RA patients is not clarified. Therefore, further clinical trials are needed to validate our findings acquired from mouse models. In addition, our findings indicated that MES inhibit the OC differentiation through inhibiting the NF-κB pathway; however, the components with therapeutic effects in MES which contain over 160 proteins remain unclear. Regarding the potential of MES for developing biological agents, further study is needed to identify the specific protein(s) in MES that exert immunoregulatory functions for the treatment of inflammatory bone erosion.

STAR★METHODS

Detailed methods are provided in the online version of this paper and include the following:

- KEY RESOURCES TABLE
- RESOURCE AVAILABILITY
  - Lead contact
  - Materials availability
  - Data and code availability
- EXPERIMENTAL MODEL AND SUBJECT DETAILS
  - Ethics approval and consent to participate
  - Mice
  - RA patients
  - Creation of a mouse model of CIA
  - Cell culture and reagents
  - *T. spiralis* and MES preparation
- METHOD DETAILS
  - Micro-CT analysis of the joints
  - Tartrate-resistant acid phosphatase (TRAP) staining
  - Generation of OCs *in vitro*
  - Western blotting
  - Real-time reverse transcription-quantitative polymerase chain reaction (RT-qPCR)
  - Multiplex immunofluorescence staining
  - Cytokine assay
  - Flow cytometry
- QUANTIFICATION AND STATISTICAL ANALYSIS

SUPPLEMENTAL INFORMATION

Supplemental information can be found online at https://doi.org/10.1016/j.isci.2022.103979.

ACKNOWLEDGMENTS

We thank Ms. Xiaoxue Xu (Core facility center, Capital Medical University) for flow cytometry analysis advice. This work was supported by grants from the National Natural Science Foundation of China (81572016, 81672042) and Beijing Natural Science Foundation (7162017, 7202008).

AUTHOR CONTRIBUTIONS

X.P.Z. and Y.L.C. conceived the work. Y.L.C., X.P.Z., and B.Z. designed experiments. Y.Y., Q.H.Z., Y.L.C., S.Q.D., Y.Q.L., and J.J.H. conducted experiments and analyzed data. L.W. provided patient samples. J.F.H. performed fluorescence immunoassay. Y.L.C. and Y.Y. prepared the original draft. X.P.Z., B.Z., and Y.L.C. edited the manuscript. All authors reviewed and approved the final version prior to submission.

DECLARATION OF INTERESTS

The authors declare that no competing interests exist.

Received: September 28, 2021
Revised: January 19, 2022
Accepted: February 18, 2022
Published: March 18, 2022

REFERENCES

Atri, C., Guerfali, F.Z., and Laouini, D. (2018). Role of human macrophage polarization in inflammation during infectious diseases. Int. J. Mol. Sci. *19*. https://10.3390/ijms19061801.

Barranco, C. (2016). Experimental arthritis: helminth infection ameliorates arthritis. Nat. Rev. Rheumatol. *12*, 373. https://10.1038/nrrheum.2016.95.

Boyle, W.J., Simonet, W.S., and Lacey, D.L. (2003). Osteoclast differentiation and activation. Nature *423*, 337–342. https://10.1038/nature01658.

Catrina, A.I., Svensson, C.I., Malmstrom, V., Schett, G., and Klareskog, L. (2017). Mechanisms leading from systemic autoimmunity to joint-specific disease in rheumatoid arthritis. Nat. Rev. Rheumatol. *13*, 79–86. https://10.1038/nrrheum.2016.200.

Chen, Z., Andreev, D., Oeser, K., Krljanac, B., Hueber, A., Kleyer, A., Voehringer, D., Schett, G., and Bozec, A. (2016). Th2 and eosinophil responses suppress inflammatory arthritis. Nat. Commun. *7*, 11596. https://10.1038/ncomms11596.

Cheng, Y., Zhu, X., Wang, X., Zhuang, Q., Huyan, X., Sun, X., Huang, J., Zhan, B., and Zhu, X. (2018). Trichinella spiralis infection mitigates collagen-induced arthritis via programmed death 1-mediated immunomodulation. Front.Immunol. *9*, 1566. https://10.3389/fimmu.2018.01566.

Choe, J.Y., Park, K.Y., Park, S.H., Lee, S.I., and Kim, S.K. (2013). Regulatory effect of calcineurin inhibitor, tacrolimus, on IL-6/sIL-6R-mediated RANKL expression through JAK2-STAT3-SOCS3 signaling pathway in fibroblast-like synoviocytes. Arthritis Res. Ther. *15*, R26. https://10.1186/ar4162.

Doonan, J., Lumb, F.E., Pineda, M.A., Tarafdar, A., Crowe, J., Khan, A.M., Suckling, C.J., Harnett, M.M., and Harnett, W. (2018). Protection against arthritis by the parasitic worm product ES-62, and its Drug-Like small molecule analogues, is associated with inhibition of osteoclastogenesis. Front.Immunol. *9*, 1016. https://10.3389/fimmu.2018.01016.

Douglas, B., Oyesola, O., Cooper, M.M., Posey, A., Tait, W.E., Giacomin, P.R., and Herbert, D.R. (2021). Immune system investigation using parasitic helminths. Annu. Rev. Immunol. *39*, 639–665. https://10.1146/annurev-immunol-093019-122827.

Fernandes, T.L., Gomoll, A.H., Lattermann, C., Hernandez, A.J., Bueno, D.F., and Amano, M.T. (2020). Macrophage: a potential target on cartilage regeneration. Front.Immunol. *11*, 111. https://10.3389/fimmu.2020.00111.

Fukui, S., Iwamoto, N., Takatani, A., Igawa, T., Shimizu, T., Umeda, M., Nishino, A., Horai, Y., Hirai, Y., Koga, T., et al. (2017). M1 and m2 monocytes in rheumatoid arthritis: a contribution of imbalance of M1/M2 monocytes to osteoclastogenesis. Front.Immunol. *8*, 1958. https://10.3389/fimmu.2017.01958.

Han, C., Yu, J., Zhang, Z., Zhai, P., Zhang, Y., Meng, S., Yu, Y., Li, X., and Song, M. (2019). Immunomodulatory effects of Trichinella spiralis excretory-secretory antigens on macrophages. Exp. Parasitol. *196*, 68–72. https://10.1016/j.exppara.2018.10.001.

Harris, N.L., and Loke, P. (2017). Recent advances in type-2-cell-mediated immunity: insights from helminth infection. Immunity *47*, 1024–1036. https://10.1016/j.immuni.2017.11.015.

Italiani, P., and Boraschi, D. (2014). From monocytes to M1/M2 macrophages: phenotypical vs. Functional differentiation. Front.Immunol. *5*, 514. https://10.3389/fimmu.2014.00514.

Kay, J., and Upchurch, K.S. (2012). ACR/EULAR 2010 rheumatoid arthritis classification criteria. Rheumatology (Oxford) *51*, i5–i9. https://10.1093/rheumatology/kes279.

Khan, Y.A., Maurya, S.K., Kulkarni, C., Tiwari, M.C., Nagar, G.K., and Chattopadhyay, N. (2020). Fasciola helminth defense molecule-1 protects against experimental arthritis by inhibiting osteoclast formation and function without modulating the systemic immune response. Faseb J. *34*, 1091–1106. https://10.1096/fj.201901480RR.

Kim, J.H., and Kim, N. (2014). Regulation of NFATc1 in osteoclast differentiation. J. Bone Metab. *21*, 233–241. https://10.11005/jbm.2014.21.4.233.

Kobpornchai, P., Flynn, R.J., Reamtong, O., Rittisoonthorn, N., Kosoltanapiwat, N., Boonnak, K., Boonyuen, U., Ampawong, S., Jiratanh, M., Tattiyapong, M., and Adisakwattana, P. (2020). A novel cystatin derived from Trichinella spiralis suppresses macrophage-mediated inflammatory responses. PLoS Negl. Trop. Dis. *14*, e8192. https://10.1371/journal.pntd.0008192.

Lee, J.W., Hoshino, A., Inoue, K., Saitou, T., Uehara, S., Kobayashi, Y., Ueha, S., Matsushima, K., Yamaguchi, A., Imai, Y., and Iimura, T. (2017). The HIV co-receptor CCR5 regulates osteoclast function. Nat. Commun. *8*, 2226. https://10.1038/s41467-017-02368-5.

Lechner, A., Bohnacker, S., and Esser-Von, B.J. (2021). Macrophage regulation & function in helminth infection. Semin.Immunol. *53*, 101526. https://10.1016/j.smim.2021.101526.

Lorenzo, J. (2017). The many ways of osteoclast activation. J. Clin. Invest. *127*, 2530–2532. https://10.1172/JCI94606.

Luo, J., Yang, Z., Ma, Y., Yue, Z., Lin, H., Qu, G., Huang, J., Dai, W., Li, C., Zheng, C., et al. (2016). LGR4 is a receptor for RANKL and negatively regulates osteoclast differentiation and bone resorption. Nat. Med. *22*, 539–546. https://10.1038/nm.4076.

Mbalaviele, G., Novack, D.V., Schett, G., and Teitelbaum, S.L. (2017). Inflammatory osteolysis: a conspiracy against bone. J. Clin. Invest. *127*, 2030–2039. https://10.1172/JCI93356.

Mcdonald, M.M., Khoo, W.H., Ng, P.Y., Xiao, Y., Zamerli, J., Thatcher, P., Kyaw, W., Pathmanandavel, K., Grootveld, A.K., Moran, I., et al. (2021). Osteoclasts recycle via osteomorphs during RANKL-stimulated bone resorption. Cell *184*, 1940. https://10.1016/j.cell.2021.03.010.

Nevius, E., Gomes, A.C., and Pereira, J.P. (2016). Inflammatory cell migration in rheumatoid arthritis: a comprehensive review. Clin. Rev. Allergy Immunol. *51*, 59–78. https://10.1007/s12016-015-8520-9.

Ono, T., and Nakashima, T. (2018). Recent advances in osteoclast biology. Histochem.Cell Biol. *149*, 325–341. https://10.1007/s00418-018-1636-2.

Orecchioni, M., Ghosheh, Y., Pramod, A.B., and Ley, K. (2019). Macrophage polarization: different gene signatures in M1(LPS+) vs. Classically and M2(LPS-) vs. Alternatively activated macrophages. Front.Immunol. *10*, 1084. https://10.3389/fimmu.2019.01084.

Radovic, I., Gruden-Movsesijan, A., Ilic, N., Cvetkovic, J., Mojsilovic, S., Devic, M., and Sofronic-Milosavljevic, L. (2015). Immunomodulatory effects of Trichinella spiralis-derived excretory-secretory antigens. Immunol. Res. *61*, 312–325. https://10.1007/s12026-015-8626-4.

Redpath, S.A., Fonseca, N.M., and Perona-Wright, G. (2014). Protection and pathology during parasite infection: IL-10 strikes the balance. Parasite Immunol. *36*, 233–252. https://10.1111/pim.12113.

Rolot, M., and Dewals, B.G. (2018). Macrophage activation and functions during helminth infection: recent advances from the laboratory mouse. J. Immunol.Res. *2018*, 2790627. https://10.1155/2018/2790627.

Saraiva, M., and O'Garra, A. (2010). The regulation of IL-10 production by immune cells. Nat. Rev. Immunol. *10*, 170–181. https://10.1038/nri2711.

Sarter, K., Kulagin, M., Schett, G., Harris, N.L., and Zaiss, M.M. (2017). Inflammatory arthritis and systemic bone loss are attenuated by gastrointestinal helminth parasites. Autoimmunity *50*, 151–157. https://10.1080/08916934.2016.1261837.

Schett, G., and Gravallese, E. (2012). Bone erosion in rheumatoid arthritis: mechanisms, diagnosis

and treatment. Nat. Rev. Rheumatol. *8*, 656–664. https://10.1038/nrrheum.2012.153.

Schopf, L.R., Hoffmann, K.F., Cheever, A.W., Urban, J.J., and Wynn, T.A. (2002). IL-10 is critical for host resistance and survival during gastrointestinal helminth infection. J. Immunol. *168*, 2383–2392. https://10.4049/jimmunol.168.5.2383.

Scott, D.L., Wolfe, F., and Huizinga, T.W. (2010). Rheumatoid arthritis. Lancet *376*, 1094–1108. https://10.1016/S0140-6736(10)60826-4.

Sobotkova, K., Parker, W., Leva, J., Ruzkova, J., Lukes, J., and Jirku, P.K. (2019). Helminth therapy - from the parasite perspective. Trends Parasitol. *35*, 501–515. https://10.1016/j.pt.2019.04.009.

Song, C., Yang, X., Lei, Y., Zhang, Z., Smith, W., Yan, J., and Kong, L. (2019). Evaluation of efficacy on RANKL induced osteoclast from RAW264.7 cells. J. Cell. Physiol. *234*, 11969–11975. https://10.1002/jcp.27852.

Steinfelder, S., O'Regan, N.L., and Hartmann, S. (2016). Diplomatic assistance: can Helminth-Modulated macrophages act as treatment for inflammatory disease? PLoS Pathog. *12*, e1005480. https://10.1371/journal.ppat.1005480.

Tardito, S., Martinelli, G., Soldano, S., Paolino, S., Pacini, G., Patane, M., Alessandri, E., Smith, V., and Cutolo, M. (2019). Macrophage M1/M2 polarization and rheumatoid arthritis: a systematic review. Autoimmun.Rev. *18*, 102397. https://10.1016/j.autrev.2019.102397.

Tunyogi-Csapo, M., Kis-Toth, K., Radacs, M., Farkas, B., Jacobs, J.J., Finnegan, A., Mikecz, K., and Glant, T.T. (2008). Cytokine-controlled RANKL and osteoprotegerin expression by human and mouse synovial fibroblasts: fibroblast-mediated pathologic bone resorption. Arthritis Rheum. *58*, 2397–2408. https://10.1002/art.23653.

Udalova, I.A., Mantovani, A., and Feldmann, M. (2016). Macrophage heterogeneity in the context of rheumatoid arthritis. Nat. Rev. Rheumatol. *12*, 472–485. https://10.1038/nrrheum.2016.91.

Wang, Z., Hao, C., Zhuang, Q., Zhan, B., Sun, X., Huang, J., Cheng, Y., and Zhu, X. (2020). Excretory/Secretory products from trichinella spiralis adult worms attenuated DSS-Induced colitis in mice by driving PD-1-Mediated m2 macrophage polarization. Front.Immunol. *11*, 563784. https://10.3389/fimmu.2020.563784.

Yang, Y., Liu, L., Liu, X., Zhang, Y., Shi, H., Jia, W., Zhu, H., Jia, H., Liu, M., and Bai, X. (2020). Extracellular vesicles derived from trichinella spiralis muscle larvae ameliorate TNBS-Induced colitis in mice. Front.Immunol. *11*, 1174. https://10.3389/fimmu.2020.01174.

STAR★METHODS

KEY RESOURCES TABLE

REAGENT or RESOURCE	SOURCE	IDENTIFIER
Antibodies		
PerCP anti-mouse/human CD11b Antibody	Biolegend	Cat#101229; RRID:AB_2129375
Alexa Fluor® 488 anti-mouse CD115 (CSF-1R) Antibody	Biolegend	Cat#135512; RRID:AB_11218983
CD206 (MMR) Monoclonal Antibody (MR6F3), APC, eBioscience™	invitrogen	Cat#17-2061-82; RRID:AB_2637420
F4/80 Monoclonal Antibody (BM8), FITC, eBioscience™	invitrogen	Cat# 11-4801-82; RRID:AB_2637191
iNOS Monoclonal Antibody (CXNFT), PE, eBioscience™	ebioscience	Cat#12-5920-82; RRID:AB_2572642
PE Rat IgG2a, κ Isotype Ctrl Antibody	Biolegend	Cat#400507; RRID:AB_326530
Rat IgG2b kappa Isotype Control (eB149/10H5), APC, eBioscience™	ebioscience	Cat#17-4031-81; RRID:AB_470175
CD14 Monoclonal Antibody (61D3), APC-eFluor 780, eBioscience™	ebioscience	Cat#47-0149-42; RRID:AB_1834358
CD68 Monoclonal Antibody (eBioY1/82A (Y1/82A)), PE, eBioscience™	ebioscience	Cat#12-0689-42; RRID:AB_10805746
BD Horizon™ BV421 Mouse Anti-Human CD192 (CCR2)	BD	Cat#564067; RRID:AB_2738573
Anti-F4/80 antibody [CI:A3-1]	Abcom	Cat#ab6640; RRID:AB_1140040
Anti-Mannose Receptor antibody	Abcom	Cat#ab64693; RRID:AB_1523910
Anti-iNOS antibody	Abcom	Cat#ab15323; RRID:AB_301857
Goat Anti-Rabbit IgG H&L (HRP)	Abcom	Cat#ab6721; RRID:AB_955447
Mounting Medium With DAPI - Aqueous, Fluoroshield	Abcom	Cat#ab104139
NF-κB p65 (D14E12) XP® Rabbit mAb	Cell Signaling Technology	Cat#8242; RRID:AB_10859369
Phospho-NF-κB p65 (Ser536) (93H1) Rabbit mAb	Cell Signaling Technology	Cat#3033; RRID:AB_331284
IκBα (44D4) Rabbit mAb	Cell Signaling Technology	Cat#4812; RRID:AB_10694416
Phospho-IκBα (Ser32) (14D4) Rabbit mAb	Cell Signaling Technology	Cat#2859; RRID:AB_561111
Phospho-SAPK/JNK (Thr183/Tyr185) (81E11) Rabbit mAb	Cell Signaling Technology	Cat#4668; RRID:AB_823588
p38 MAPK (D13E1) XP® Rabbit mAb	Cell Signaling Technology	Cat#8690; RRID:AB_10999090
Phospho-p38 MAPK (Thr180/Tyr182) (D3F9) XP® Rabbit mAb	Cell Signaling Technology	Cat#4511; RRID:AB_2139682
Phospho-p44/42 MAPK (Erk1/2) (Thr202/Tyr204) (D13.14.4E) XP® Rabbit mAb	Cell Signaling Technology	Cat#4370; RRID:AB_2315112

(*Continued on next page*)

Continued

REAGENT or RESOURCE	SOURCE	IDENTIFIER
p44/42 MAPK (Erk1/2) (L34F12) Mouse mAb	Cell Signaling Technology	Cat#4696; RRID:AB_390780
SAPK/JNK Antibody	Cell Signaling Technology	Cat#9252; RRID:AB_2250373
Phosphoto-SAPK/JNK (Thr183/Tyr185) (81E11) Rabbit mAb	Cell Signaling Technology	Cat#4668; RRID:AB_823588
NFAT1 (D43B1) XP® Rabbit mAb	Cell Signaling Technology	Cat#5861; RRID:AB_10834808
β-Actin (13E5) Rabbit mAb	Cell Signaling Technology	Cat#4970; RRID:AB_2223172
IRDye 800CW Goat anti-Rabbi	Li-cor	Cat#926–32211 RRID:AB_621843
Chemicals, peptides, and recombinant proteins		
Immunization Grade BovineType II Collagen	Chondrex	Cat#20022
Complete Freund's Adjuvant	Chondrex	Cat#7001
Incomplete Freund's Adjuvant	Chondrex	Cat#7002
Mouse 1× Lymphocyte Separation Medium	DAYOU	Cat#7211011
Histopaque®-1083	Sigma-Aldrich	Cat#10831-100ML
Lipopolysaccharide (LPS) Solution (500X)	invitrogen	Cat#00-4976-93
Recombinant Murine IL-4	PeproTECH	Cat#214-14
Recombinant Murine sRANK Ligand (E.coli derived)	PeproTECH	Cat#315-11
Recombinant Murine M-CSF	PeproTECH	Cat#315-02
Recombinant Human M-CSF	PeproTECH	Cat#300-25
Recombinant Human sRANK Receptor	PeproTECH	Cat#310-08
RIPA	Solarbio	Cat#R0010
Protease inhibitor ,Cocktail ,50x	APPLYGEN	Cat#P1265
IC Fixation Buffer	invitrogen	Cat#00-8222-49
10×Permeabilization Buffer	invitrogen	Cat#88-17000-210
Critical commercial assays		
Human IL-10 Precoated ELISA Kit	DAYOU	Cat#1111002
Human IL-6 Precoated ELISA Kit	DAYOU	Cat#1110603
Human IL-1 β Precoated ELISA Kit	DAYOU	Cat#1110123
Human TNF-α Precoated ELISA Kit	DAYOU	Cat#1117202
IL-6 Mouse Uncoated ELISA Kit	Invitrogen	Cat#88-7064-88
IL-1 beta Mouse Uncoated ELISA Kit	Invitrogen	Cat#88-7013-88
TNF alpha Mouse Uncoated ELISA Kit	Invitrogen	Cat# 88-7324-77
IL-10 Mouse Uncoated ELISA Kit	Invitrogen	Cat# 88-7105-88
Pierce™ BCA Protein Assay Kit	Thermo Scientific	Cat#23227
ProcartaPlex multiplex protein assays	Thermo Scientific	N/A
Opal 7-Color Manual IHC Kit	PerkinElmer	Cat#NEL811001KT
Experimental models: Cell lines		
RAW264.7	BMCR	http://cellresource.cn/contact.aspx
Experimental models: Organisms/strains		
ICR mice	The Jackson Laboratory	RRID:IMSR_JAX:009122
DBA/1 mice	Mouse Genome Informatics	RRID:MGI:2159837

(*Continued on next page*)

Continued

REAGENT or RESOURCE	SOURCE	IDENTIFIER
C57BL/6J	The Jackson Laboratory	RRID:IMSR_JAX:000664
T. spiralis	This paper	ISS 533
RA patients and healthy donors	Beijing Friendship hospital, Capital Medical University	N/A
Oligonucleotides		
Primers for RT-qPCR, see Table S3	This paper	N/A
Software and algorithms		
mimics	Materialise	http://biomedical.materialise.com/mimics
Image J	National Institutes of Health	https://imagej.net/
Prism 9.0	GraphPad	http://www.graphpad.com/

RESOURCE AVAILABILITY

Lead contact

Further information and requests for resources and reagents should be directed to and will be fulfilled by the lead contact, Prof. Xinping Zhu (zhuxping@ccmu.edu.cn).

Materials availability

This study did not generate new unique reagents.

Data and code availability

- This study did not generate new sequencing data, and data reported in this paper will be shared by the lead contact upon request.
- This paper does not report original code.
- Any additional information required to reanalyze the data reported in this paper is available from the lead contact upon request.

EXPERIMENTAL MODEL AND SUBJECT DETAILS

Ethics approval and consent to participate

This study was performed in accordance with the recommendations of the Institutional Review Board (IRB) of Capital Medical University. All animal experimental procedures were approved by the Animal Care and Use Committee of Capital Medical University (approval number: AEEI-2016-008) and complied with the National Institutes of Health Guidelines for the Care and Use of Experimental Animals. The clinical study was performed in accordance with the Declaration of Helsinki and was approved by the IRB of Capital Medical University (approval number: 2016SY01).

Mice

Male DBA/1 mice, 8–10 weeks old, and male C57BL/6J mice 6–8 weeks old, were purchased from the Laboratory Animal Services Center of Capital Medical University (Beijing, China).

RA patients

A total of 26 patients with RA (male/female = 4/22) requiring medication from Beijing Friendship Hospital were enrolled from March to May 2021. The diagnosis of RA was made according to ACR/EULAR 2010 RA classification criteria (Kay and Upchurch, 2012). All clinical information was collected based on the protocol approved by the IRB. Written informed consent was provided by all the patients with a promise of identity protection. Blood samples from 20 healthy donors (male/female = 8/12) were used as controls in this study.

Creation of a mouse model of CIA

Male DBA/1 mice were used to generate a model of CIA following a previously described method (Cheng et al., 2018). Briefly, bovine type II collagen (CII) (Chondrex, Redmond, WA, USA) was dissolved in 0.01 M acetic acid at a concentration of 2 mg/mL by stirring overnight at 4°C and emulsified with an equal volume of complete Freund's adjuvant (Chondrex). Male DBA/1 mice were intradermally immunized at the base of the tail with 0.1 mL of emulsion containing 100 μg of CII followed by a booster comprising the same amount of CII emulsified with incomplete Freund's adjuvant on day 21. To evaluate the therapeutic effect of *T. spiralis* infection on CIA in mice, a total of 15 mice were divided into three groups (n = 5 mice per group), namely, an CIA group, in which CIA was induced by CII immunization; a *T. spiralis*-infected group, in which mice were infected with 400 infective *T. spiralis* muscle larvae 14 days before the first CII immunization; and a control group, in which mice did not receive any treatment. To evaluate the therapeutic effect of MES on CIA in mice, a total of 15 mice were also divided into three groups (n = 5 mice per group), namely, an CIA group; an intraperitoneal injection of protein group, in which mice were treated via the intraperitoneally injection route with 20 μg/mice of MES on day −2, 0, 21 and 28 of the first CII immunization; and a control group.

Cell culture and reagents

Mouse or human PBMCs were isolated from blood by density gradient centrifugation using Histopaque-1083 solution (Sigma, USA). To induce macrophages, the collected PBMCs were cultured in complete α-MEM (Gibco, Carlsbad, CA, USA) containing 10% heat-inactivated fetal bovine serum (FBS) (Gibco, Carlsbad, CA, USA) and 1% penicillin–streptomycin for 3hat 37°C with 5% CO_2 in a humidified incubator. Non-adherent cells were removed and the culture medium was replaced with complete α-MEM supplemented with 30 ng/mL M-CSF (Peprotech, USA) for 3 days for macrophage induction.

Peritoneal cells from mice were collected from the peritoneal cavities of mice from each group by lavage with 10 mL of Ca^{2+}- and Mg^{2+}-free Hanks' balanced salt solution (HBSS). The cells were centrifuged at 500 ×*g* for 10minat 4°C and then seeded in 6-well plates in RPMI 1640 (Gibco) supplemented with 10% heat-inactivated FBS and 1% penicillin–streptomycin for 4 h, followed by the collection of the adherent cells (macrophages).

Mouse bone marrow cells (BMCs) were isolated from 6-8-week-old C57BL/6J WT mice by flushing femoral and tibia bones with HBSS containing 10% heat-inactivated FBS. BMCs were plated in 24-well plates (5×10^5/well) in complete α-MEM medium with M-CSF (30 ng/mL) for 3 days and then the non-adherent cells were removed and adherent bone marrow-derived macrophages (BMMs) were harvested to induce OCs. The culture medium containing M-CSF (30 ng/mL) was replaced every 2 days.

All the hind paws from mice were collected, and the skin was removed, and the paws were fixed in 4% paraformaldehyde. After 48 h, they were decalcified in 0.5% formaldehyde and 20% EDTA for 4 weeks until they became pliable. Then, the paws were embedded in paraffin and sectioned.

The RAW 264.7 murine macrophages were obtained from the Chinese National Infrastructure of Cell Line Resource (http://cellresource.cn/contact.aspx, China). The cells were cultured in complete DMEM medium at 37°C with 5% CO2 in a humidified incubator.

T. spiralis and MES preparation

The *T. spiralis* ISS 533 strain was maintained in female ICR mice as previously described (Wang et al., 2020). To collect excretory/secretory products of *T. spiralis* muscle larvae (MES), muscle larvae were collected from the muscles of ICR mice infected with 400 infective *T. spiralis* larvae for 50 days using pepsin digestion (Wang et al., 2020). The collected larvae were cultured in serum-free RPMI 1640 medium (Phenol Red-free, Thermo Fisher, Carlsbad, CA, USA) containing 2% penicillin–streptomycin at 37°C and with 5% CO2 for 48 h. The culture supernatants were collected and concentrated by centrifugation at 3,000 rpm for 50 min, the buffer was changed to PBS, which was followed by filtration using an Amicon Centrifugal Filter (Millipore) with a MWCO of 3 KD. The MES concentration was measured by BCA assay and the contents were identified by SDS–PAGE.

METHOD DETAILS

Micro-CT analysis of the joints

Micro-CT was performed on the hind paws of mice from all the groups (numbers of mice n = 5 each) using a Bruker SkyScan 1276 Micro-CT Scanner (SkyScan, Antwerp, Belgium). Scanning was done at 70 kV, 142 mA,

using a 1-mm aluminum filter at a resolution of 8 μm. Three-dimensional microstructural parameters were calculated using Mimics Software (Materialise, Belgium) to observe bone erosion. The bone volume/total volume ratio (BV/TV) and trabecular thickness (Tb.Th) were measured using CTAn Software (Bruker, Brussels, Belgium) (Luo et al., 2016).

Tartrate-resistant acid phosphatase (TRAP) staining

TRAP staining was performed to identify OCs using the naphthol-based method as previously described (Lee et al., 2017). The hind paws of the mice were fixed in 4% formaldehyde for 48 h, and then decalcified in 0.5% formaldehyde and 20% EDTA for 4 weeks until they became pliable. The paws were embedded in paraffin and sectioned. After being de-waxed, the sections were placed in 0.1 M $CaCl_2$-$MgCl_2$ solution overnight for 19 h to pre-activate the TRAP enzyme, stained using a TRAP staining kit (Sigma–Aldrich, Saint Louis, MO, USA) at 37°C for 1 h, and counterstained with hematoxylin. Osteoblasts were identified as $TRAP^+$ multinucleated cells (nuclei number ≥ 3) adjacent to bone (Luo et al., 2016) and images were captured using ImageJ software.

Generation of OCs *in vitro*

Macrophages can be induced to multinucleated $TRAP^+$ OCs under incubation with RANKL (Song et al., 2019). Macrophages induced by mouse or human PBMCs were incubated in 48-well plates (3×10^4 cells per well) in complete α-MEM containing 30 ng/mL M-CSF and 50 ng/mL murine RANKL (Peprotech, USA) for 7 days to stimulate OCs differentiation. The differentiated OCs were identified by TRAP straining.

To observe the effect of M1 polarization on OC differentiation from macrophages, RAW264.7 cells were incubated in complete DMEM in the presence of LPS (100 ng/mL) or IL-4 (20 ng/mL). After 6 h, 50 ng/mL RANKL was added to induce OC differentiation.

To observe the effect of MES on OC differentiation from macrophages, RAW264.7 cells or BMMs were incubated in complete DMEM in the presence of MES (4, 8, and 16 μg/mL). After 2 h, 100 ng/mL LPS was added to induce M1 polarization for 6 h, followed by the addition of 50 ng/mL RANKL for 5–7 days to induce OC differentiation.

Western blotting

Total protein was extracted from OCs induced from RAW264.7 cells using ice-cold radioimmunoprecipitation assay (RIPA) lysis buffer (Cell Signaling Technology, Beverly, MA, USA) containing 1 mM phenylmethylsulfonyl fluoride (PMSF). Protein concentrations were measured using a BCA assay kit. Equal amounts of protein were separated by 12% SDS–PAGE, transferred onto polyvinylidene difluoride (PVDF) membranes, blocked with 5% skimmed milk in Tris-buffered saline (TBS) containing 0.05% Tween 20 (TBST) for 1 h, incubated with primary antibodies against the major downstream signaling molecules involved in osteoclastogenesis, namely, phosphorylated (p)-NF-κB p65 (Ser536), total NF-κB p65, p-IκB-α (Ser32), total IκB-, p-p44/42 MAPK (ERK1/2) (Thr202/Tyr204), total p44/42 MAPK (ERK1/2), p-p38 MAPK (Thr180/Tyr182), total p38 MAPK, p-SAPK/JNK (Thr183/Tyr185), total SAPK/JNK, and NFAT1 (all from Cell Signaling Technology; diluted 1:1,000) in TBST overnight at 4°C, and then with IRDye 800CW-conjugated anti-rabbit IgG (Li-COR, Lincoln, NE, USA) for 1hat room temperature. Beta-actin served as the control. The protein bands were visualized using an Odyssey CLx Infrared Imaging System.

Real-time reverse transcription-quantitative polymerase chain reaction (RT-qPCR)

Total RNA was extracted from snap-frozen synovial tissue of the hind paw joints or OCs induced from mouse PBMCs or RAW264.7 cells using Trizol Reagent (Sigma). The extracted RNA was reverse-transcribed into cDNA using SuperscriptIII RT (Vazyme, China) according to the manufacturers' instructions. qPCR was performed in an Applied Biosystems QuantStudio 5 Real-Time PCR System (Thermo Fisher Scientific, USA) using an AceQ Universal SYBR qPCR Master Mix (Vazyme, China). The relative mRNA levels of NFAT, MMP-9, c-Fos, TRAP, Cath K, RANK, IL-1β, IL-6, IL-12, TNF-α, INOS, MCP-1, Arg-1, CD206, and IL-10 were normalized to that of the reference gene *GAPDH* and quantified using the $2^{-\Delta\Delta Ct}$ method. The sequences of the primers used in the qPCR are listed in Table S3.

Multiplex immunofluorescence staining

Paraffin-embedded sections of mouse hind paw tissue were de-waxed, followed by heat-induced antigen retrieval in EDTA (pH = 9.0) using a microwave oven. After blocking for 1 h with goat serum (ZhongShan

JinQiao-Bio, China), the sections were incubated with primary antibodies targeting F4/80, CD206, and NOS2 (all from Abcam, London, UK) for 1hat room temperature, and then with an HRP-conjugated secondary antibody (Abcam). Detection was performed using the Opal Multiplexed Manual IHC Kit (PerkinElmer, USA). Finally, all the sections were counterstained with DAPI, sealed, and observed and recorded using a Vectra Polaris imaging system (PerkinElmer, USA). Staining was analyzed using inForm Cell Analysis software (PerkinElmer, USA).

Cytokine assay

To determine the effect of *T. spiralis* infection on inflammatory cytokine production in mice with CIA, the serum cytokine profile was analyzed with the Procarta Plex Multi-factor Immunoassay Kit (26 factors) (Invitrogen, USA) using Luminex xMAP technology following the manufacturer's instructions. To detect the cytokines secreted by peritoneal macrophages, peritoneal macrophages collected from mice of the different groups were stimulated with 100 ng/mL LPS for 6 h for M1 polarization, following which the levels of secreted cytokines in the culture supernatants were measured by cytokine-specific ELISA according to the manufacturer's instructions (eBioscience, San Diego, CA, USA). To determine the effect of *T. spiralis* MES on inflammatory cytokine production in monocytes derived from PBMCs of RA patients, purified monocytes were pre-incubated with 4 μg/mL MES for 2 h before stimulation with 100 ng/mL LPS for 6 h. Cytokine levels in the culture supernatants were subsequently measured by ELISA (eBioscience). To determine the effects of MES on macrophage polarization, RAW264.7 cells were pre-incubated with different concentrations (4, 8, or 12 μg/mL) of MES for 2 h before stimulation with 100 ng/mL LPS or 20 ng/mL IL-4 for 6 h, after which cytokine levels in the culture supernatants were measured by ELISA.

Flow cytometry

For cell surface staining, peritoneal macrophages were stained with anti-mouse F4/80 (FITC) and anti-mouse CD11b (eFluor 450); mouse PBMCs were stained with anti-mouse CD115 (Alexa Flour 488) and anti-mouse CD11b; and human blood monocytes were stained with anti-human CD14 (APC-eFluor 780) and anti-human CCR2 (BV421). The corresponding isotype antibodies were used as controls in the presence of CD16/32 to block FcγR binding for 30minat 4°C in the dark. For intracellular staining, cells were fixed in IC Fixation Buffer and permeabilized using permeabilization buffer (both from Invitrogen). Then, mouse PBMCs and peritoneal macrophages were incubated with anti-mouse CD206 (APC) and anti-mouse NOS2 (PE-conjugated), while human blood monocytes were incubated with anti-human CD68 (PE-conjugated) or their isotype controls for 50minat room temperature in the dark. Flow cytometry was performed using a Flow Cytometer (BD, NJ, USA) and analyzed using FlowJo Software. The gates were set based on isotype and/or fluorescence-minus-one controls in all experiments. All antibodies were purchased from Thermo Fisher (Carlsbad, USA).

QUANTIFICATION AND STATISTICAL ANALYSIS

Statistical analysis was performed using GraphPad Prism 7. All data are shown as means ± SEM. Paired or unpaired Student's t-tests were used for comparison between two groups. ANOVA was performed for comparisons among multiple groups. A p-value <0.05 was considered significant.